vetmeduni

Department of Biomedical Sciences

University of Veterinary Medicine Vienna

Institute of Pharmacology and Toxicology

(Head: Univ.-Prof. Dr.med.univ Veronika Sexl)

Understanding brachyury genetics and developing strategies to target brachyury in chordoma

Master Thesis

University of Veterinary Medicine Vienna

Submitted by

Kerstin Kornelson, BSc

External Supervisor

Professor Paul Workman FRS FmedSci

Internal Supervisor

Karoline Kollmann, PhD

Reviewer

Dr. Heidi Neubauer

Declaration of authorship:

I declare that this Master Thesis has been written by myself. I have not used any other than the listed sources, nor have I received any unauthorized help.

I hereby certify that I have not submitted this Master Thesis in any form (to a reviewer for assessment) either in Austria or abroad.

Furthermore, I assure that the (printed and electronic) copies I have submitted are identical.

Date: 13.02.2023 Signature: .....

Acknowledgements

First and foremost, I want to thank my external supervisor Prof. Paul Workman, for welcoming me into his lab and allowing me to learn so much from this exciting project in chordoma research. I am very thankful for all the scientific support and guidance.

Special thanks to my mentor Dr. Hadley Sheppard who was there to support me in the lab and taught me everything from cell culture techniques to CRISPR-Cas9 gene editing. I am very grateful for all the great advice on how to plan, conduct, analyse and present scientific research, with the goal of becoming an independent scientist. It was very sad to hear that you were leaving the ICR, as I really enjoyed the time in the lab with you, but I felt well prepared to complete the rest of the project under the new circumstances.

I would also like to thank my internal supervisor Dr. Karoline Kollmann for her support and availability from miles away during this project.

At this point I want to thank the lab team who have been so welcoming and always willing to help me from the beginning. Many thanks to Dr. Paul Clarke for all the useful scientific guidance during the weekly meetings and anytime in between. I also want to thank Rachel and Kate, for always willing to lend a hand, especially with the shipping of the cells to the US.

Next, I want to thank the CRIS Cancer Foundation for supporting this research project through a donation.

I also want to thank the lab teams of the Structural genomics consortium in Chapel Hill and Oxford, as well as the Chordoma Foundation for all their efforts in our brachyury drug discovery collaboration.

I am eternally grateful to my lovely family, including my mom, dad, my brother Erik and my grandparents. Thanks for all the support, for always having an open ear and the fun days in London this summer.

I am thankful for all my friends, who always support me, no matter how far away I was, for spending hours on facetime with me and for visiting me in London.

Finally, I want to thank my partner Fabian, who accompanied me to London and really made this experience to one of the best in my life. Thanks for building me up whenever I was in doubt, for your unconditional support and the unforgettable time in London.

Abstract

Chordoma is a rare primary bone cancer that is dependent on the expression of the transcription factor brachyury (*T*). To better understand the drivers of this cancer, the chordoma associated SNP rs2305089, was investigated in nine chordoma cell lines and two non-chordoma cell lines. Sanger sequencing revealed that the SNP variant only occurs in chordoma cell lines and mostly in a homozygous form. It was not found in the non-chordoma cell lines sequenced. This data confirms the association of the SNP rs2305089 with chordoma.

Chordomas are largely resistant to conventional chemotherapies and are prone to recurrence and metastasis despite surgical removal and radiotherapy, the current standard of care. Therefore, the development of a targeted therapy is of utmost importance. Brachyury is considered as the ideal therapeutic target as it is minimally present in healthy tissues yet chordoma cells require it to grow. This work provides evaluation of novel compounds intended to selectively inhibit brachyury. These inhibitors were tested in cell-based assays focusing on their impact on brachyury protein levels, cell viability, the induction of senescence and target engagement. The two most promising covalent compounds CF-8-70 and CF-8-137 modulate brachyury, induce senescence, and are less toxic than other analogues. Washout of these inhibitors maintained cellular senescence, which is the phenotypic outcome of selective brachyury inhibition. Moving forward, as the covalent compounds bind to a specific cysteine residue on the brachyury protein, a serine mutant was engineered using CRISPR-Cas9. This mutant cell line allows further improvement of compound selectivity for brachyury.

Compared to developing a brachyury selective chemical probe, transcriptional CDK inhibition represents an immediately actionable approach to treat chordoma. The *T* gene is driven by a super enhancer and this regulation confers sensitivity to inhibitors of transcriptional CDK. This thesis adds to the evaluation of the clinical-grade transcriptional CDK inhibitor fadraciclib on its ability to modulate brachyury in chordoma cells and *in vivo*. Chordoma cells show sensitivity to fadraciclib and treatment successfully depletes brachyury protein levels. In addition, the determination of a maximum tolerated dose in a CH22 xenograft mouse model was started. However, no reduction in brachyury protein levels was achieved with the administered dose in this study.

Zusammenfassung

Das Chordom ist ein seltener primärer Knochenkrebs, der von der Expression des Transkriptionsfaktors Brachyury (*T*) abhängig ist. Um die Genetik dieser Krebsart besser zu verstehen, wurde der mit dem Chordom assoziierte SNP rs2305089 in neun Chordom-Zelllinien und zwei Nicht-Chordom-Zelllinien untersucht. Die durchgeführte Sanger-Sequenzierung ergab, dass der SNP nur in Chordom-Zelllinien vorkommt, wo er meist homozygot vorliegt. In den sequenzierten Nicht-Chordom-Zelllinien wurde er nicht gefunden. Diese Ergebnisse bestätigen den Zusammenhang zwischen dem SNP rs2305089 und dem gehäuften Auftreten von Chordomen.

Chordome sind weitgehend resistent gegen Chemotherapien und neigen trotz chirurgischer Entfernung und Strahlentherapie zu Rückfällen und Metastasenbildung. Daher ist die Entwicklung einer zielgerichteten Therapie von größter Bedeutung. Brachyury wird als ideales therapeutisches Ziel angesehen, da es in gesundem Gewebe kaum vorhanden ist und für das Wachstum von Chordom-Zellen essenziell ist. Im Rahmen dieser Masterarbeit wurden neuartige Verbindungen untersucht, die Brachyury selektiv hemmen sollen. Diese Inhibitoren wurden in zellbasierten Assays getestet, wobei der Schwerpunkt auf ihren Auswirkungen auf den Brachyury-Proteinspiegel, die Lebensfähigkeit der Zellen, die Induktion von Seneszenz und die Binding an Brachyury innerhalb der Zelle liegt. Die beiden vielversprechendsten kovalenten Verbindungen CF-8-70 und CF-8-137 inhibieren Brachyury, induzieren Seneszenz und sind weniger toxisch als andere Analoga. Selbst nach Entfernung dieser Inhibitoren blieb die zelluläre Seneszenz erhalten, die das phänotypische Ergebnis einer selektiven Brachyury-Hemmung widerspiegelt. Da die kovalenten Verbindungen an einen spezifischen Cysteinrest des Brachyury-Proteins binden, wurde mithilfe von CRISPR-Cas9 eine Serin-Mutante generiert. Diese mutierte Zelllinie ermöglicht die Selektivität der Verbindungen für Brachyury zu überprüfen und zu verbessern.

Während der Entwicklung selektiver Brachyury-Hemmer, könnten transkriptionelle CDK-Hemmer eine unmittelbare Möglichkeit zur Behandlung des Chordoms darstellen. Teil dieser Masterarbeit ist die Evaluierung des CDK-Hemmers Fadraciclib in Chordomzellen und *in vivo*. Es konnte bestätigt werden, dass Chordomzellen empfindlich gegenüber Fadraciclib sind und gleichzeitig die Brachyury inhibiert wird. Darüber hinaus wurde mit der Bestimmung einer maximal tolerierten Dosis *in vivo* begonnen. Jedoch wurde in dieser Studie mit der verabreichten Dosis keine Senkung des Brachyury-Proteinlevels erzielt.

List of abbreviations

ATCC	American Type Culture Collection
BSA	Bovine Serum Albumin
CDK	Transcriptional cyclin-dependent kinase
CNV	Copy number variation
DMSO	Dimethylsulfoxid
EA	Enzyme acceptor
EGFR	Epidermal growth factor receptor
EMT	Epithelia-mesenchymal-transition
ePI	ProLabel
FBS	Fetal bovine serum
HAT	Histone acetyltransferasess
HDAC	Histone deacetylases
HDR	Homology directed repair
HRP	Horseradish peroxidase
PBS	Phosphate-buffered saline
PD	Pharmacodynamics
PDGFRB	Platelet-derived growth factor receptor beta
PDX	Patient derived xenograft
PK	Pharmacokinetics
PROTACS	Proteolysis targeting chimeras
pSer2 RNA pol II	Phosphorylated Serine 2 of RNA pol II
pSer5 RNA pol II	Phosphorylated Serine 5 of RNA pol II
RT-qPCR	Reverse transcription quantitative real-time PCR
SGC	Structural Genomics Consortium
SNP	Single nucleotide polymorphism
STR	Short tandem repeat

TAE	Tris-acetate-EDTA
TBS	Tris-buffered saline

Key terms

Brachyury

CDK inhibitor

Chordoma

CRISPR-Cas9

SNP

Transcription factor

Table of content

1. Introduction

1.1. Chordoma

Chordoma is a malignant notochordal tumour of the skull base, mobile spine and sacrum that was first described by Virchow in 1857 (1). These tumours presumably derive from undifferentiated remnants of the notochord, an embryonic structure that coordinates cell fate and development. This is based on the fact that brachyury, a transcription factor required for notochord development, is aberrantly expressed in chordomas (2).

Due to the rarity of the disease, efforts to identify the molecular basis of chordoma have been limited in the past. The Chordoma Foundation was established in 2007 to revitalise efforts by bringing together researchers from all areas of chordoma research. By creating a biobank for the distribution of bio specimens, cell line and patient derived xenograft (PDX) repositories, and drug screening programmes to collaborate with researchers and validate therapeutic candidates, the Chordoma Foundation has ensured that working on this rare cancer is now feasible.

1.1.1. Epidemiology of the disease

Chordoma occurs with an annual incidence of 0.8 per 1,000,000 in Europe and the USA, roughly equivalent to 350 cases per year (3,4). Approximately 1-4 % of all bone malignancies are chordomas (5). It may occur in all age groups, but mostly affects people in their fifth to seventh decade of life with a clear predominance of cases in men (4,5). Due to the disease's rarity, epidemiological studies that have examined chordoma incidence and survival patterns have primarily used small case series or combined it with other uncommon bone neoplasms.

Chordoma can arise anywhere along the spine and historically, it was thought to occur more frequently in the pelvic bones than the base of the skull (6). A comprehensive epidemiology study of 400 histologically confirmed chordoma cases between the period of 1973-1995 revealed almost equal distribution among skull base, mobile spine and sacrum. Among that cohort, 32 % of the cases were cranial, 32.8 % were spinal, and 29.2 % were sacral (7). Female sex and young age (< 26 years) were linked to a higher incidence of cranial presentation according to that study (7). The 5-year, 10-year, and 20-year survival rates decline to 67.6%, 39.9%, and 13.1%, respectively, with a median survival of about 6 years (7,8).

A small subset of chordomas is discovered to run in families, even though the majority of chordomas occur sporadically (9). Familial inheritance cases of chordoma are rare and tend to affect younger patients (under 40 years). Furthermore, these tumours occur more commonly in the clival region (10).

1.1.2. Classification

The pathological diagnosis and sub-categories of chordoma have evolved as more knowledge about the disease has been gained. The WHO fifth edition classifies three subtypes of chordoma as conventional and/or chondroid, poorly differentiated and dedifferentiated (11). Each subtype has its unique epidemiology, treatment regimen, and clinical course.

Conventional/chondroid chordoma

Approximately 95 % of all cases are conventional chordomas (12). This subtype primarily affects adults and is occurs more frequently in males than females, most commonly in the sacral region of the spine. Histologically, these tumours have a chondroid appearance similar to chondrosarcomas (13). Expression of nuclear brachyury is the diagnostic hallmark of conventional and chondroid chordoma (2).

Poorly differentiated chordoma

This rare subtype primarily occurs in paediatrics with an average age of 10 years. It is more commonly located in the clivus, skull base and cervical spine and shows a slight female predominance (14). Poorly differentiated chordomas grow faster and are more aggressive than the conventional and chondroid subtype (15). These tumours are histologically described to share similarities with conventional chordoma with aggressive nuclear pleomorphism (16). Immunohistochemically, it can be distinguished through complete SMARCB1/INI1 loss while still expressing brachyury and cytokeratin (14).

Dedifferentiated chordoma

Dedifferentiated chordoma only occur in approximately 2-8 % of cases with an average age of 57 years (17). It is slightly more frequent in males and mostly arises in the sacral region (17).

About half of dedifferentiated chordomas occur at recurrence of a prior conventional chordoma (17). This subtype grows the fastest and is more likely to metastasize (18). It is histologically described to have high-grade sarcoma features, increased mitoses and loss of brachyury and cytokeratin within the dedifferentiated part (17).

1.1.3. Symptoms and therapeutic options

The symptoms of chordoma are highly dependent on the individual location of the tumour (16). Accordingly, patients with sacral chordomas may complain of back pain, urinary and bowel dysfunction and neuropathy. Clival location may cause headaches, diplopia or other cranial dysfunction (16). Due to slow tumour growth, nonspecific symptoms and unfamiliarity of clinicians with this rare disease, diagnosis can be delayed several months to years (16).

The clinical management of the disease is challenging due to the positioning of chordomas along important bone and neurological structures. To date, surgical resection of the tumour and radiation therapy are the standard of care (19). Local recurrences and metastases occur in 40 % of cases, diminishing the average lifespan after chordoma diagnosis to 5-7 years (20). Aggressive surgery with wide margins can prevent local recurrences (21), but may result in poor patient outcome by risking considerably higher morbidity due to possible injuring of the sacral nerve.(22). In most cases, surgery is combined with radiation therapy, which can improve local control and survival rates of chordoma patients (16).

When considering systemic therapy, it is important to distinguish between the different chordoma subtypes. While conventional and/or chondroid chordomas are largely considered chemotherapy-resistant, the poorly differentiated and/or dedifferentiated subtypes are sensitive to it (16). Cytotoxic chemotherapy is an essential part of treatment of the poorly differentiated and dedifferentiated chordomas (16).

Apart from brachyury, very few molecular drivers are known for chordoma (16). Nevertheless, recurrent alterations or overexpression in genes such as epidermal growth factor receptor (EGFR), chromatin regulator SMARCB1 and platelet-derived growth factor receptor beta (PDGFRB) are known in this type of tumour (16). Chordoma cells were not responsive to

clinically approved PDGFRB inhibitors like sunitinib and imatinib (23), however EGFR inhibitors displayed activity in chordoma cells with different potency (16,23).

Due to the lack of an approved systemic therapy to treat chordoma, there is an urgent need for the development of a targeted therapy. Searching for a target that can be appropriate for all chordoma tumours, the transcription factor brachyury is considered as the most promising candidate according to the current state of chordoma research. Compared to other transcription factors, brachyury is minimally expressed in healthy adult tissues and found in virtually all chordomas (2). The fact that chordoma cells require the expression of brachyury to survive (24) **(Fig. 1)** has led to brachyury being referred to as the "Achilles heel" of chordoma. Therefore, a better understanding of its genetics and the development of strategies to target brachyury in chordoma is truly necessary.

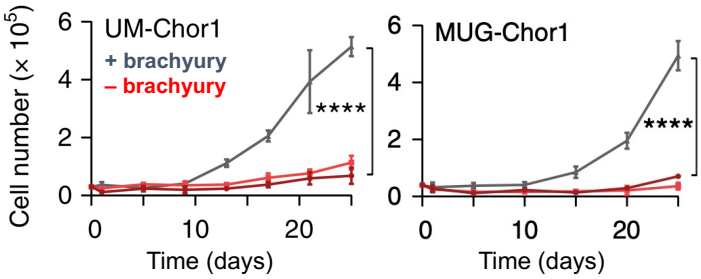

Fig. 1: *T* (brachyury) is essential for chordoma cells to survive. Reduction in chordoma cell proliferation induced by sgRNA-mediated brachyury repression (red). Image adapted from reference (24).

1.2. Brachyury

The T-box developmental transcription factor brachyury was the first of this family to be discovered in 1927 (25). Brachyury is encoded by the *T* gene, where the letter *T* stands for “tailless”. This refers to the tailless phenotype resulting from heterozygous loss-of-function mutations in mice (25). The role of brachyury has historically been studied in the context of embryonic development. During gastrulation, the three primary germ layers – ectoderm, mesoderm and endoderm – gradually move to create the structure of the primitive streak. As a transcription factor, brachyury is responsible for activating the movements of cells down the primitive streak via a process known as epithelia-mesenchymal-transition (EMT) (26). The mesoderm gives rise to the notochord, which is later replaced by the spinal cord during embryonic

development (27). *T* is critical for the establishment of the anterior-posterior axis and notochord differentiation (28). In the mouse embryo, brachyury is turned on at day 7.5 and expressed in the primitive streak, tailbud, and notochord before turning off at day 13 (29). After that day, brachyury is only minimally expressed in healthy mature tissues including the pituitary gland and testes (30). Since complete deletion of the *T* gene in all examined organisms causes embryonic lethality, brachyury is indispensable for the development of vertebrates (31).

1.2.1. Brachyury structure

In humans, the brachyury encoding *T* gene is located on chromosome 6q27 and is approximately 10 kb in length. The human *T* was first cloned from foetal intervertebral discs in 1996 and this revealed a high degree of protein sequence conservation with other vertebrate *T* homologs, especially in the DNA binding domain (32). The transcription factor brachyury is located in the nucleus and built up of a large DNA-binding domain as well as the activation and repression domains (32). The DNA-binding domain (T-box) is located in the N-terminal portion of the gene and binds to the sequence TCACACCT in a dimerized form. The T-box binding domain of *T* has been crystalized using the *Xenopus laevis* Xbra (33) and recently human brachyury (34) **(Fig. 2)**.

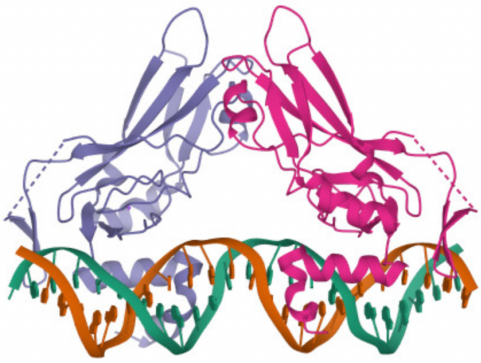

Fig. 2: Crystallography structure of human brachyury bound to DNA duplex as a dimer. Violet and pink ribbons denote T-box domain. Image from reference (34).

While the T-box domain of brachyury is quite well explored, the C-terminus is yet to be characterized. The C-terminus has two sets of activation and repression domains that enable activation and repression of transcription (35). Analysis of the protein coding sequence of brachyury has shown that the C-terminal half of brachyury is intrinsically disordered, similar to many TFs (36). Regions that are intrinsically disordered lack a stable three-dimensional structure

and hence cannot be crystalized. These regions exhibit a low proportion of hydrophobic, bulky amino acids and a high content of charged, polar amino acids (37). Based on these traits, it is assumed that inherently disordered transcription factors, such as brachyury, can attain high specificity for their target binding sequences with low affinity. As a result, brachyury can regulate a number of target genes that are necessary for chordoma cells to survive (38).

1.2.2. Role in diseases

Brachyury contributes to a variety of diseases. Variants in the *T* gene have been linked to an increased risk of developing neural tube defects such as spina bifida (39). Within the context of cancer, brachyury has been shown to be expressed in more than 40 % of primary lung carcinomas but is not required for its tumorigenesis (40). Brachyury has been identified as a driver of EMT in human carcinomas (41). EMT has been implicated to favour invasiveness, metastatic dissemination and drug resistance of tumour cells (42). Therefore, brachyury plays a role in lung cancer metastasis (40) and is associated with higher risk of recurrence and distant metastasis of breast cancer (42).

1.2.3. Brachyury in chordoma

In chordomas, brachyury plays a significantly important role. Chordoma tumours show differentiation towards the notochord, hence they may arise from notochordal remnants (43). The notochord is a midline embryonic structure that is required for chordate development. It expresses numerous orthologues of the transcription factors brachyury and FoxA which are important for its differentiation and developmental function (44). Vertebral and skull-based chordomas were assumed to arise from the notochordal cells due to their similar morphology, immunophenotype and anatomical position (45). Cell tracking has confirmed that isolated notochordal cells can remain as remnants in murine vertebral columns (46). The link between the notochord and chordoma was clearly demonstrated at a molecular level when microarray studies of gene expression showed consistent, specific mRNA expression of *T* in chordomas. The expression of *T* is considered as the diagnostic hallmark of chordoma. Immunohistochemical detection of brachyury has proven to be crucial for chordoma diagnosis and to differentiate it from tumours with similar histology (47).

1.2.4. Genetic variation and familial chordoma

Genetic variation is an important source of evolutionary and phenotypic diversity, although in many cases contributes to the risk of developing complex diseases such as cancer. Single nucleotide polymorphisms (SNPs) and copy number variations (CNVs) are two of the most common types of genetic variation that have been extensively studied. The allele frequency of a genetic mutation in the population serves as the definition of a SNP. Common polymorphisms are variations that occur in more than 1 % of the population, whereas rare polymorphisms have a minor allele frequency of 0.1-1 %. CNVs are relatively common variable regions of the genome larger than 1 kb which contain losses or gains of DNA. Deletions and duplications of numerous cancer genes have been linked with increased cancer risk (48). It has been shown that germline variants within the coding region of a gene may alter protein coding and hence influence its function. For example, the DNA damage repair genes *BRCA1* and *BRCA2* are associated with hereditary breast cancer and ovarian cancer syndrome (49). Germline variants of *PALB2*, the partner and localizer of *BRCA2*, are involved in increased risk of developing breast, ovarian and pancreatic cancer (50).

In chordoma, high-resolution array-CGH in familial chordoma patients has identified a region on 6q27 as a susceptibility determinant in these families (10). The region on 6q27 only contains the *T* gene. Tandem duplication of this gene in the germline is linked to increased susceptibility of developing the familial form of chordoma (10) but is not observed in sporadic cases (51).

1.2.5. The chordoma associated brachyury SNP

A strong association between chordoma risk and the common nonsynonymous SNP rs2305089 was observed in Europeans by Pillay et al. (52). This variant leads to a substitution of glycine by an aspartic amino acid at amino acid 177 (Gly177Asp) at exon 4 of the *T* gene. Among the chordoma patients studied, 97 % had at least one allele of the mutation (52). Furthermore, a higher mRNA expression of *T* was found in patients with AA genotype than in the heterozygous GA genotype (52). The SNP is also common in the general population, as around half of individuals harbour it on at least one allele (53). Interestingly, SNP rs2305089 was not significantly associated with chordoma risk among the Chinese population (54). However, a very recent study confirmed the linkage of the SNP with chordoma risk within a cohort of the Iranian population (55), which suggests that the reported association seems to be related to different ethnic populations.

Rs2305089 is located within the DNA binding domain in the highly conserved T-box of *T* and alters the binding ability of the transcription factor (53). Brachyury binds to its target DNA as a homodimer. The Asp-177 variant does not prevent binding of brachyury to the DNA, however it appears to reduce the stability of the formed *T* dimer (53).

1.2.6. Genetic regulation in chordoma

In general, transcription factors are proteins that bind DNA helices at certain regulatory sequences to either activate or inhibit gene transcription through a trans-activation or trans-repression domain. Transcription starts with the RNA polymerase binding to the promoters of DNA molecules. Transcriptional regulation is controlled by transcription factors through binding to certain DNA sequences to recruit RNA polymerase II initiation or elongation factors (56). In the promoter region, transcription initiation sites can be found. Additionally, some DNA sequences that are positioned close to or far from promoter regions have several transcription factor binding sites. These DNA sequences are known as "enhancers" and promote higher levels of gene expression (57). Large clusters of enhancers in close genomic proximity are defined as super-enhancers. In normal cell types, super enhancers are cell type specific and regulate genes that are important for cell identity (58). However, many oncogenes are regulated by super enhancers, such as *MYC* in neuroblastoma (59) or *RARA* in AML (60).

Brachyury is a super enhancer driven master transcription factor that defines gene programs associated with chordoma identity (38). Master transcription factors frequently regulate one another by forming a transcription factor core regulatory circuitry to define cell identity (61). In chordoma, brachyury regulates and is regulated by transcription factors including MYC, NR3C1, ID1, HoxA and HoxB (38). In primary chordoma patient tissue and chordoma cell lines, high brachyury expression is maintained through a super-enhancer in close proximity to the *T* gene (24). Brachyury autoregulates through binding its super-enhancer and forming a transcriptional condensate at the *T* locus **(Fig. 3)** (38). It binds many promotors and enhancers of target genes that are enriched with its T-box DNA-binding motifs (24). Super enhancers like that regulating brachyury contain remarkably high levels of RNA polymerase II and non-coding RNA (61). Trough introducing a single transcription factor binding site within a typical enhancer, said super enhancers can be formed, indicating that these regulatory components are fairly cooperative (59). Mutually, perturbation of co-factors or deletion of their genetic elements can

lead to the breakdown of the entire super enhancer. In chordoma cells, selective degradation of brachyury disrupts brachyury autoregulation and induces senescence (38).

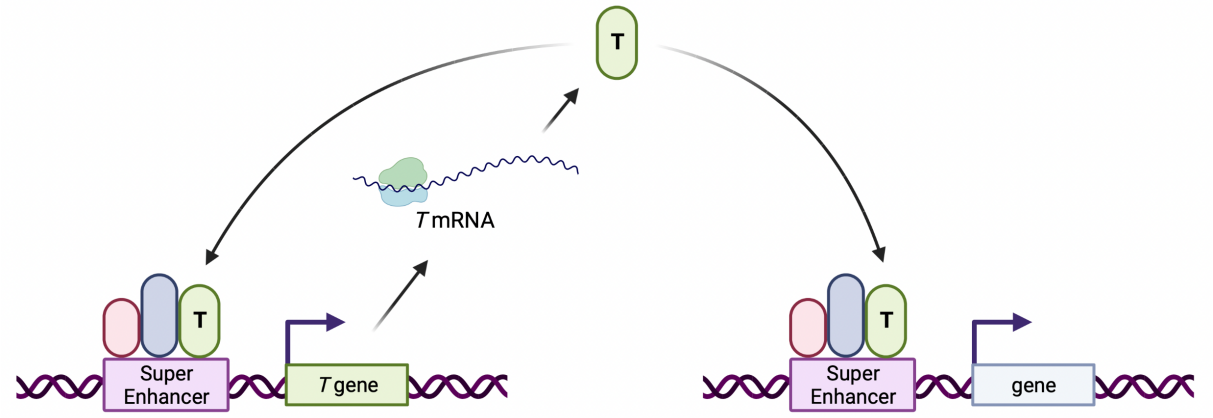

Fig. 3: Schematic of brachyury autoregulatory life cycle. Image adapted from reference (24) and created with BioRender.com.

1.3. Targeting transcription factors in cancer

Transcription factor deregulation is a hallmark of cancer and approximately 40 % of known oncogenes and tumour suppressors are either transcription factors or directly act on the transcription cycle (62). The first transcription factors to be identified as oncogenic were fusion proteins that occur in various leukaemia subtypes (63). However, oncogenic transcription factors were historically considered undruggable (64). This was due to the difficulties associated with targeting their protein-protein or protein-DNA interactions that mediate their function, in comparison to more accessible active sites of enzymes or kinases. Protein-protein interaction surfaces are normally flatter and lack the deep binding pockets of enzyme active sites, which complicates the development of small-molecule inhibitors (65). This has led to an urgent unmet clinical need to therapeutically address cancers defined by transcription factor deregulation.

Over the past years, numerous transcription factors were identified and validated, whose dysregulation plays a key role in cancer **(Tab. 1)**. At the same time, the number of approaches for modulating the activity of transcription factors has been considerably expanded (66). As an example, there are recent advances in developing degraders of the Ikaros family of transcription factors, which are key drivers of multiple myeloma (67) and clinical success modulating the nuclear hormone family of transcription factors (68). Several new innovations to target

transcription factors have been investigated including cysteine reactive inhibitors targeting intrinsically disordered regions of transcription factors or the usage of proteolysis targeting chimeras (PROTACS) (66). A bifunctional PROTAC molecule consists of a ligand (usually a small molecule inhibitor) of the protein of interest and a covalently bound ligand of an E3 ubiquitin ligase. After binding to the protein, PROTAC can recruit E3 to ubiquitinate the protein, which is then proteasomally degraded (69). Nevertheless, most oncogenic transcription factors are not yet therapeutically targetable with drugs.

Tab. 1: Examples of transcription factors playing a key role in cancer. Adapted from source (66).

Cancer	Transcription factors
Acute myeloid leukaemia	MLL-AF9, CBFβ–SMMHC, CBFβ–SMMHC, RUNX1-ETO, CBFβ, RUNX1, p53
Acute promyelocytic leukaemia	PML-RAPα
Breast cancer	SIX1, RUNX2, FOXO
Gastric cancer	KLF8
Glioblastoma	GABP
Hepatocellular carcinoma	MYC
Lymphoma	MYC
Melanoma	RUNX2, STAT1
Prostate cancer	RUNX2
T-cell acute lymphoblastic leukaemia	TAL1, CATA3, RUNX1

1.4. Therapeutic strategies to target brachyury

1.4.1. Development of direct brachyury inhibitors or degraders

Given the importance of brachyury in chordoma and its absence in most adult tissues, this protein is considered the most promising target for developing a systemic treatment for the disease. Recently it was shown that direct pharmacological targeting of brachyury induces senescence in chordoma cells and inhibits chordoma identity genes (38). Despite the challenges that come with the structure of transcription factors, a number of chemical fragments capable to bind to brachyury could be identified by the teams of Dr. David Drewry at the University of North Carolina, Dr. Opher Gileadi at the University of Oxford, and Dr. Charles Lin at Baylor College of Medicine. Eight potential binding pockets were found in Oxford by x-ray crystallography fragment screening using crystals of brachyury. The identified crystalized fragments served as starting point for the development of brachyury inhibiting or degrading compounds (70).

Simultaneously with the fragment-based discovery effort, the development and evaluation of compounds derived from afatinib is underway. Afatinib [Giotrif (EU) or Gilotrif (USA)] is an irreversible inhibitor of the ErbB family of tyrosine kinases that covalently binds to all homo- and heterodimers formed by ErB3, ErB4, Her2 and EGFR (71). Giotrif is approved for the treatment of non-small cell lung cancer (NSCLC) with activating EGFR mutations or advanced squamous NSCLC after platinum-based chemotherapy (72).

In various chordoma cell lines, treatment with afatinib revealed depletion of brachyury levels (23) and *in vivo* experiments showed potent tumour growth inhibition in xenograft mouse models (23). Recently, the Gileadi group was able to show on the basis of crystal structures, that afatinib can bind to the brachyury DNA binding domain **(Fig. 4B)**, specifically to Cysteine 122 (73). Moving further, compounds with measurable affinities were identified by Surface Plasmon Resonance (SPR) (74), optimizing the binding affinity of new covalent compounds targeting Cysteine 122 and simultaneously reducing the binding affinity towards EGFR is in progress. In parallel, potential candidates are being investigated in cell lines at the ICR in London, which is part of the effort in this master thesis.

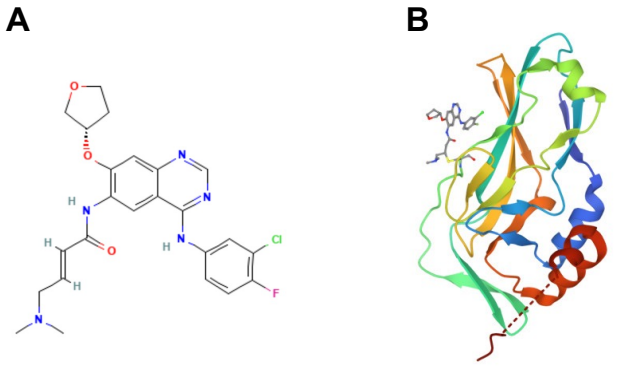

Fig. 4: Developing compounds derived from afatinib. (A) Afatinib compound structure. (B) Crystal structure of afatinib in complex with brachyury. Images from sources (73,75).

1.4.2. Transcriptional brachyury inhibition in chordoma

It has been shown that oncogenic master transcription factors like brachyury can be downregulated by inhibitors of the transcriptional and chromatin machinery (38). This was achieved for the first time with Myc oncogenes, which were downregulated by inhibitors of the Bromodomain and Extra-Terminal (BET) family of acetyl-lysine reader transcriptional co-activators (76). A number of malignancies have shown comparable responses to treatment in subsequent investigations using pharmacological inhibitors of transcriptional cyclin-dependent kinases (CDKs) (77), histone acetyltransferases (HATs) (78) and histone deacetylases (HDACs) (79).

Simultaneously to the time-consuming efforts of developing a brachyury inhibitor or degrader, the evaluation of clinical grade transcriptional CDK inhibitors in context of brachyury is ongoing. In chordoma, *T* is the most highly expressed super enhancer-associated transcription factor (80). Recently, screening of 459 small molecules in chordoma cells revealed the most significant reduction in cell proliferation by inhibitors of CDK7/12/13 and CDK9 (24). It was found that treatment with the transcriptional CDK7/12/13 inhibitor THZ1 leads to preferential downregulation of brachyury in chordoma cell lines and a significant tumour-suppressive effect in a xenograft mouse model (24). This indicates that brachyury autoregulation is sensitive to transcriptional CDK inhibition.

As transcriptional CDK inhibition provides a potential therapeutic opportunity to downregulate brachyury, this thesis deals with the further evaluation of the clinical candidate fadraciclib (formerly CYC065) in the context of chordoma. The transcriptional CDK2 and CDK9 inhibitor fadraciclib was developed at the Institute of Cancer Research London (ICR) in collaboration with Cyclacel Pharmaceuticals. The inhibitor is currently in phase 1/2 clinical studies in patients with advanced solid tumours or lymphoma (81) and leukaemia or myelodysplastic syndrome (82). Fadraciclib was designed by further optimization from the first-generation parent compound seliciclib and has significantly improved metabolic stability, efficacy and potency (83). CDK2 is a key cell cycle regulator, promotes DNA replication and is involved in DNA damage response (84,85). CDK9 is a major regulator of RNA polymerase II meditated transcription of genes critical for proliferation, survival and cell cycle regulation (86). Fadraciclib treatment decreases levels of RNA polymerase II C-terminal domain serine 2 phosphorylation (pSer2 RNA pol II), MCL1 and MYC oncoproteins, that are downstream effectors of CDK9 (83). Thereby, rapid apoptosis is induced in cancer cells (83).

1.5. Problem statement and aim of this thesis

Chordomas are resistant to conventional chemotherapies (4) and show a high tendency of recurrence and metastasis despite surgical excision and radiation therapy (20). Therefore, targeted chordoma therapeutics are urgently needed. The transcription factor brachyury is expressed in virtually all chordoma tumours (87) and is not present in most adult tissues (2). Brachyury is crucial for cell survival and proliferation of chordoma cells (88) and its knock down induces growth arrest (39). These findings make brachyury the most important target to treat chordoma. The chordoma associated SNP variant rs2305089 (G117D) of the brachyury *T* gene is present in over 90 % of chordomas (52). Less is known about the functional consequences of the SNP in chordoma cells. Therefore, this thesis deals with the investigation of the SNP in different chordoma cell lines and non-chordoma cell lines and motivates to further examine the genomic differences it in these cells.

Transcription factors such as brachyury have been considered undruggable in the past due to their lack of deep binding pockets, which make it more challenging to develop small molecules (65). Efforts to drug transcription factor dependent cancers are under way and recently it has become apparent that overcoming these structural challenges is no longer an impossibility.

This thesis aims to improve and evaluate novel brachyury binding compounds in cell-based assays.

Furthermore, it was recently demonstrated that the T gene is driven by a super enhancer and that this regulation confers sensitivity to inhibitors of transcriptional CDKs (24,38). The evaluation of the clinical-grade transcriptional CDK inhibitor fadraciclib in chordoma cells and *in vivo* is part of this thesis. Efforts in this thesis will contribute to the development of a chordoma targeted therapy and advance to development strategies to drug transcription factor dependent cancers.

1.5.1. Hypotheses and research questions

To advance the understanding of the chordoma associated SNP in chordoma cells, this hypothesis and question will be verified:

1. The chordoma associated SNP (G177D) is present in chordoma cell lines and cannot be found in brachyury of non-chordoma cell lines.

- Is the SNP homozygous or heterozygous in different chordoma cell lines?

In order to identify ways to target brachyury activity via indirect or direct inhibition, the following hypotheses and research questions are to be addressed in this thesis:

2. Brachyury can be directly targeted by small molecules.

- Do the compounds bind to brachyury in living cells?
- Do brachyury protein levels deplete in chordoma cells after treatment with the compound?
- Do the compounds induce growth arrest in cells?
- Do the compounds induce senescence in chordoma cells?

3. Brachyury can be indirectly targeted by the transcriptional CDK inhibitor fadraciclib.

- Do brachyury protein levels deplete after treatment?
- Does the combination with senolytic agents induce apoptosis in chordoma cells?
- Does fadraciclib modulate brachyury *in vivo*?

2. Materials and Methods

2.1. Chemicals, reagents and kits

Tab. 2: Chemicals and reagents.

Manufacturer	Chemicals and reagents	Cat. No.
Bethyl Laboratories, USA	Rabbit anti-RNA Polymerase II Phospho (S2) antibody	A300-654A
	Rabbit anti-RNA Polymerase II Phospho (S5) antibody	A304-408A
Cell Signaling Technology, USA	Anti-rabbit IgG, HRP-linked Antibody	7074
	Blue Loading Buffer	7722
	Brachyury (D2Z3J) Rabbit mAb	81694
	GAPDH (D4C6R) Mouse mAb	97166
	Keratin 8/18 (C51) Mouse mAb	4546
	Mcl-1 (D2W9E) Rabbit mAb	94296
	PARP (46D11) Rabbit mAb	9532
	Vinculin (E1E9V) XP Rabbit mAb	13901
Constituted at ICR	Dulbecco's phosphate-buffered saline (PBS)	
	Trypsin	
Integrated DNA Technologies, Inc., USA	Cas9 Nuclease	1081058
Marvel, UK	Original Dried Skimmed Milk	
Mirus Bio LLC, USA	TransIT-LT1 Transfection Reagent	MIR 2300
New England Biolabs, USA	Gel Loading Dye, Purple (6X)	B7025
	NEBuilder HiFi DNA Assembly Master Mix	E2621S
PAN-Biotech GmbH, Germany	Fetal bovine serum	P30-3306

Sigma-Aldrich, USA	Dimethyl sulfoxid	D2438
	TWEEN 20	P1379
	Formaldehyde solution, for molecular biology	F8775
Thermo Fisher Scientific, USA	Bovine Serum Albumin Powder	BP9702-100
	CellEvent Senescence Green Flow Cytometry Assay	C10840
	GeneRuler 1 kb Plus DNA Ladder	SM1331
	Gibco Cell culture media	
	Halt Protease and Phosphatase Inhibitor Cocktail 100X	78440
	Lipofectamine 3000 Transfection Reagent	L3000001
	NuPAGE™ MOPS SDS Running Buffer (20X)	NP0001
	NuPAGE™ Tris-Acetate SDS Running Buffer (20X)	LA0041
	PageRuler™ Plus Prestained Protein Ladder, 10 to 250 kDa	26619
	Phusion High-Fidelity PCR Master Mix with HF Buffer	F531L
	Pierce 20X TAE Buffer	28354
	Pierce 20X TBS Buffer	28358
	Pierce ECL Western Blotting Substrate	32109
	RIPA Lysis and Extraction Buffer	89901
	Spectra™ Multicolor High Range Protein Ladder	26625
	SYBR Safe DNA Gel Stain	S33102

T-PER Tissue Protein Extraction Reagent	78510
UltraPure Agarose	16500500
Fast SYBR Green Master Mix	4385612

Tab. 3: Kits.

Manufacturer	**Kits**	**Cat. No.**
DiscoveRX, USA	InCELL Detection Kit	96-0079
Lonza, Switzerland	MycoAlert Mycoplasma Detection Kit	LT07-218
Promega, USA	Wizard SV Genomic DNA Purification System	A2360
	Nano-Glo HiBiT Lytic Detection System	N3030
	CellTiter-Glo Luminescent Cell Viability Assay	G7570
Qiagen, Germany	RNeasy Mini Kit	74104
Thermo Fisher Scientific, USA	Neon Transfection System Kit	MPK10096
	Pierce BCA Protein Assay Kit	23225
	High-Capacity cDNA Reverse Transcription Kit	4368814
Zymo Research, USA	DNA Clean & Concentrator-5	D4004

Tab. 4: Compounds.

Manufacturer/Supplier	Compounds
Boehringer Ingelheim, Germany	Afatinib
Cyclacel Pharmaceuticals, USA	Fadraciclib
University of North Carolina, USA	CF-2-224
	CF-8-137
	CF-8-169
	CF-8-38
	CF-8-69
	CF-8-70
	CF-8-73
	CF-8-78
	UNC-AH-075D
	UNC-AH-87B
	UNC-ZDG-173-1

2.2. Cell culture

Cell lines and culture conditions

CH22 cells were provided by the Chordoma Foundation. UCH-1, UCH-2, MUG-Chor1, U-CH17M, UM-Chor1, U2OS, MUG-CC1, UM-Chor5, JHC7, SW480 and SW620 cells were obtained from American Type Culture Collection (ATCC). CH22, UM-Chor1 and U-CH1 chordoma cells were short tandem repeat (STR) profiled for cell line authentication at MD Anderson Cancer Center. The other chordoma and non-chordoma cell lines were STR profiled by the ATCC Human Cell Authentication Service. All cells were tested negative for mycoplasma using a Mycoplasma Detection Kit (MycoAlert, Lonza, Switzerland).

The CH22 cell line origins from a patient with recurrent chordoma of the sacrum and does express brachyury (89). The brachyury-expressing cell lines UCH-1, UCH-2 and MUG-Chor1 were raised from recurrent sacral chordomas (89–91). The U-CH17M cell line does express brachyury and was established from the soft tissue metastasis of a sacral chordoma (87). The cell lines UM-Chor1, MUG-CC1 and UM-Chor5 were isolated from primary clival chordomas

and express brachyury (92,93). JHC7 was established from a primary sacral chordoma and is positive for brachyury expression (94). The SW480 and SW620 cell lines were isolated from the colon of adenocarcinoma patients and are both positive for brachyury expression (95,96). The U2OS cell line was derived from a moderately differentiated osteosarcoma of the tibia and is negative for brachyury expression (97).

All cell lines were maintained on tissue-culture treated plates in respective media **(Tab. 5)** at 37 °C in humidified atmosphere containing 5 % CO_2. For freezing cells to -80 °C or to liquid nitrogen, cell pellets were resuspended in freezing media composed of 70 % respective cell culture media, 20 % fetal bovine serum (FBS) (PAN-Biotech GmbH, Germany) and 10 % Di-methyl sulfoxid (DMSO) (Sigma-Aldrich, USA).

Tab. 5: Cell culture medium compositions.

Cell line	Culture medium composition
CH22	90 % RPMI 1640 10 % fetal bovine serum (FBS)
UCH-1, UCH-2, MUG-Chor1 and U-CH17M	IMDM/RPMI (4:1) 10 % FBS 1 % L-glutamine
UM-Chor1	IMDM/RPMI (4:1) 10 % FBS
U2OS	90 % DMEM 10 % FBS
MUG-CC1	IMDM/RPMI (4:1) 10 % FBS 1 % L-glutamine 1 % ITS-G
UM-Chor5	IMDM/RPMI (4:1) 20 % FBS

	1 % 100 X MEM NEAA
JHC7	90 % DMEM:F12 10 % FBS
SW480 and SW620	90 % L-15 10 % FBS

2.3. Genotyping brachyury SNP at chr6:166579270

Genomic DNA of 9 chordoma cell lines (CH22, UCH-1, UCH-2, MUG-Chor1, U-CH17M, UM-Chor1, MUG-CC1, UM-Chor5, JHC7) and 2 non-chordoma cell lines (SW480 and SW620) was collected using a genomic DNA purification kit (Wizard SV Genomic DNA Purification System, Promega, USA) according to manufacturer's protocol.

PCR

DNA concentrations were determined using a spectrophotometer (NanoDrop ND-1000 Spectrophotometer, Thermo Fisher Scientific, USA). Samples were PCR amplified with T_SNP_Fwd and T_SNP_Rev primers **(Tab. 6)** using the Phusion High Fidelity Master mix (Thermo Fisher Scientific, USA). Reagents were mixed according to **Tab. 7**. A negative control containing water instead of DNA was carried. Amplification was performed according to the protocol in **(Tab. 8)** using a thermocycler (PTC-0225 DNA Engine Tetrad, Bio-Rad, USA). For gel electrophoresis, PCR samples and negative control were mixed 1:5 with purple gel loading dye (New England Biolabs, USA). Subsequently 5 µl of negative control, samples and GeneRuler 1kb Plus DNA ladder (Thermo Fisher Scientific, USA) were loaded on 1 % agarose gel. For the gel, 0.5 g of agarose (Thermo Fisher Scientific, USA) was dissolved in 50 ml of 1X tris-acetate-EDTA (TAE) buffer (Thermo Fisher Scientific, USA) and 5 µl of SYBR Safe DNA gel stain (Thermo Fisher Scientific, USA) were added. Gels were imaged with the ChemiDoc Imaging System (Thermo Fisher Scientific, USA). Amplified samples were purified using a PCR purification Kit (DNA Clean & Concentrator-5, Zymo Research, USA) and DNA concentration was again measured using the NanoDrop spectrophotometer. Purified PCR samples were sequenced using the sanger sequencing service provided by Source BioScience.

Tab. 6: Primers for SNP chr6:166579270 PCR.

Name	Sequence
T_SNP_Fwd	CAGAGACACTTTCTTGGGATCCAGAGGACTT
T_SNP_Rev	TTAGCGCGTCTCCCCGCTCCTCCA

Tab. 7: Reaction mix for SNP chr6:166579270 PCR.

Component	Volume per reaction
Phusion Mastermix	25 µl
Forward Primer	2.5 µl
Reverse Primer	2.5 µl
Genomic DNA	100 µg
ddH_2O	Fill up to 50 µl
Total volume per reaction	50 µl

Tab. 8: PCR amplification protocol.

Step	Temperature	Time
Initial denaturation	98 °C	30 seconds
30 cycles	98 °C 65 °C 72 °C	10 seconds 30 seconds 15 seconds
Final extension	72 °C	5 minutes
Hold	4 °C	Endless

2.4. Compound acquisition and management

CDK9/2 inhibitor Fadraciclib (CYC065) was provided by Cyclacel Pharmaceuticals. The powder was dissolved in 100 % DMSO for all *in vitro* studies at desired stock concentration and stored in aliquots at -20 °C. For *in vivo* experiments, Fadraciclib was dissolved in sterile water and stored at 4 °C.

Afatinib (Gilotrif, Boehringer Ingelheim, Germany) was purchased from Boehringer Ingelheim. Afatinib-derived brachyury-binding small molecule inhibitors were developed in collaboration with the Structural Genomics Consortium (SGC), which includes Professor David Drewry at the UNC North Carolina, Chapel Hill and SGC at the University of Oxford. The compounds were made by the Drewry group and sent to either to the ICR or SGC for testing. Crystallography and biophysical assays where accomplished at the University of Oxford. All compounds were dissolved in 100 % DMSO at desired stock concentration and stored in aliquots at -80 °C.

2.5. Western blot

To identify and quantify proteins of cells treated with the compounds of interest, western blots were accomplished. In this technique a mixture of proteins is first separated based on molecular weight and then transferred to a membrane. Incubation of the membrane with antibodies specific to the protein of interest and subsequent adding of a labelled antibody allows detection of protein specific bands. The thickness of the band corresponds to the amount of protein present (98).

Preparation of protein lysates from tissue culture

For each sample, depending on incubation time and cell line, 100,000 - 250,000 cells were seeded on 6-well plates. The compounds of interest were added to the cells on the following day. Cells were lysed in RIPA Lysis and Extraction Buffer (Thermo Fisher Scientific, USA) and protease and phosphatase inhibitors (Thermo Fisher Scientific, USA). The inhibitor was diluted with lysis buffer 1:100. 100 µl of the mixture were added to the cells and incubated for 30 minutes at 4 °C. The lysates were centrifuged for 20 minutes at 12,000 rpm at 4 °C. The protein concentration of the resulting supernatants was quantified using a BCA protein assay kit (Pierce BCA Protein Assay Kit, Thermo Fisher Scientific, USA). For the BCA, reagent A was mixed with reagent B 50:1 and 200 µl of the mixture were added to a clear 96-well plate.

10 µl lysate were added in duplicates and incubated for 30 minutes at 37 °C. Absorbance was measured at 562 nm on a plate reader (VICTOR X Multilabel Plate Reader, PerkinElmer, Inc., USA).

Preparation of protein lysates from mouse tumours

A small piece of each tumour sample was transferred to sample preparation tubes (Precellys MK28-R 2ml Hard Tissue, Bertin Instruments, France) and 200 µl of pre-cooled extraction buffer (T-PER Tissue Protein Extraction Reagent, Thermo Fisher Scientific, USA) was added to each sample. Samples were homogenized in a tissue homogenizer (Precellys 24 tissue homogenizer, Bertin Instruments, France) at 6000 rpm two times for 30 seconds. The samples were then centrifuged at 15000 rpm for 10 minutes at 4 °C and the resulting supernatant was transferred to small tubes. Protein concentration was quantified using a spectrometer (Direct Detect Spectrometer, Merck Millipore, USA).

SDS-PAGE protein electrophoresis

Protein samples were mixed 1:3 with reducing loading buffer (Blue Loading Buffer, Cell Signaling Technology, USA) and denatured for 10 minutes at 95 °C. The samples and a protein ladder for either 10-250 kDa (PageRuler, Thermo Fisher Scientific, USA) or 40-300 kDa (Spectra, Thermo Fisher Scientific, USA) were run on 4-12 % Bis-Tris gel or 3-8 % Tris-Acetate gel (NuPAGE, Thermo Fisher Scientific, USA) in MOPS or Tris-Acetate running buffer (NuPAGE, Thermo Fisher Scientific, USA) respectively, depending on the molecular weight of the protein of interest.

Transfer to membrane and antibody probing

Protein was then transferred to a nitrocellulose membrane (iBlot Transfer Stack nitrocellulose, Thermo Fisher Scientific, USA) using a western blot transfer system (iBlot 2 Dry Blotting System, Thermo Fisher Scientific, USA). Membranes were blocked in 5 % BSA in tris-buffered saline (Pierce 20X TBS Buffer, Thermo Fisher Scientific) with 0.1 % TWEEN (TWEEN 20, Sigma-Aldrich, USA) (TBST) or 5 % milk (Original Dried Skimmed Milk, Marvel, UK) in TBST buffer for one hour at room temperature. Membranes were then probed with the indicated primary antibody, each was diluted 1:1000 in 5 % BSA in TBST or 5 % milk in TBST at 4 °C overnight. Membranes were then washed 3 times with TBST for 5 minutes each. Then the

respective horseradish peroxidase (HRP) linked secondary antibody was diluted 1:2000 in 5 % BSA in TBST or 5 % milk in TBST. Membranes were incubated with secondary antibody for 1 hour at room temperature followed by another 3 wash steps with TBST for 5 minutes each. Then the detection reagent (Pierce ECL Western Blotting Substrate, Thermo Fisher Scientific, USA) was added on top of the membranes and covered with a clear plastic foil after incubating for 1 minute. The membranes were imaged with the ChemiDoc Imaging System (Bio-Rad Laboratories, USA).

2.6. Assaying cell viability

To determine the number of viable cells after incubating with compounds, a luminescent cell viability assay was accomplished (Cell-Titer Glo Luminescent Cell Viability Assay, Promega, US). The assay quantitatively measures ATP which indicates the presence of metabolically active cells. A proprietary thermostable luciferase generates a luminescent signal that is directly proportional to the amount of ATP released during the luciferase reaction.

The day before the compounds were added, 1000 cells per well of CH22 or 5000 cells of U2OS were seeded in white 96-well polystyrene plates (Corning 96-well, Cell Culture-Treated Flat-Bottom Microplate, Fisher Scientific, USA). On the next day the compounds were added to the wells. Each compound was serially diluted by a factor of 1:3 starting at a concentration of 10 µM or 50 µM and a total of 9 dilutions. DMSO was added as a control. After incubating for 6 or 7 days at 37 °C the number of viable cells was determined. Cell-Titer Glo Reagent was diluted 1:5 and 100 µl of the mixture were added to each well. After 15 minutes incubation at room temperature the luminescence signal was measured on a plate reader (VICTOR X Multilabel Plate Reader, PerkinElmer, Inc., USA). Concentration-response curves were generated using GraphPad Prism (v. 9).

2.7. Senescence assay

To investigate if the compounds induce senescence in chordoma cells, a flow cytometry assay was performed (CellEvent Senescence Green Flow Cytometry Assay, Thermo Fisher Scientific, USA). The assay is based on the cytometric detection of β-galactosidase hydrolysis. In principle, the lysosomal enzyme converts β-galactosides into monosaccharides. The CellEvent Senescence Green probe is a fluorescein-based reagent that contains two galactoside

components making it a specific target for the enzyme. The cleaved product is retained within the cell due to covalent binding of intracellular proteins and emits a fluorogenic signal that has absorption/emission maxima of 490/514 nm (99).

The day before the compounds of interest were added, 100,000 CH22 cells per sample were seeded in 6-well plates. Compounds were diluted with cell culture media to a final concentration of 1 µM and 5 µM and added to the cells in duplicates. Dilution of an equivalent volume of DMSO saved as control. After incubating for 6 days at 37 °C, the senescence assay was performed. Therefore, cells were washed with PBS on the plate, trypsinized and transferred to small tubes. After spinning down, the cells were washed with PBS twice. For fixation, the pellet was resuspended with 5 % Formaldehyde (Sigma-Aldrich, USA) in PBS and incubated for 10 minutes at room temperature protected from light. After spinning down, the pellet was washed with 1 % bovine serum albumin (BSA) (Fisher Scientific, USA) in PBS and resuspended in 100 µl of prewarmed CellEvent working solution. The pellet was subsequently resuspended in 300 µl of 1 % BSA in PBS and transferred to flow cytometer tubes. Percentage of senescent cells was analysed using a flow cytometer with a 488-nm laser and 530-nm/30 filter.

Statistical analysis

A two-tailed, unpaired *t*-test was performed to assess statistical significance of the percentage of senescence within the compound treated cells compared to the DMSO control.

2.8. InCELL target engagement assay

To validate compound binding to brachyury in a cellular environment, a thermal shift assay (InCELL Pulse Assay, DiscoveRX, USA) was performed in CH22 and U2OS cells. InCELL Pulse is based on the principle of protein thermal stability. The assay utilizes β-galactosidase enzyme split into two inactive fragments, the enhanced ProLabel (ePL) peptide and the enzyme acceptor (EA), that combine to form an active β-galactosidase enzyme. The cells are prior transfected with the protein of interest fused to ePL tag. In the next step, cells are exposed to a short heat pulse in the presence or absence of a test compound. Compound binding protects the protein from thermal denaturation which results in a gain of β-galactosidase enzyme and increase in chemiluminescent signal (100) **(Fig. 5)**.

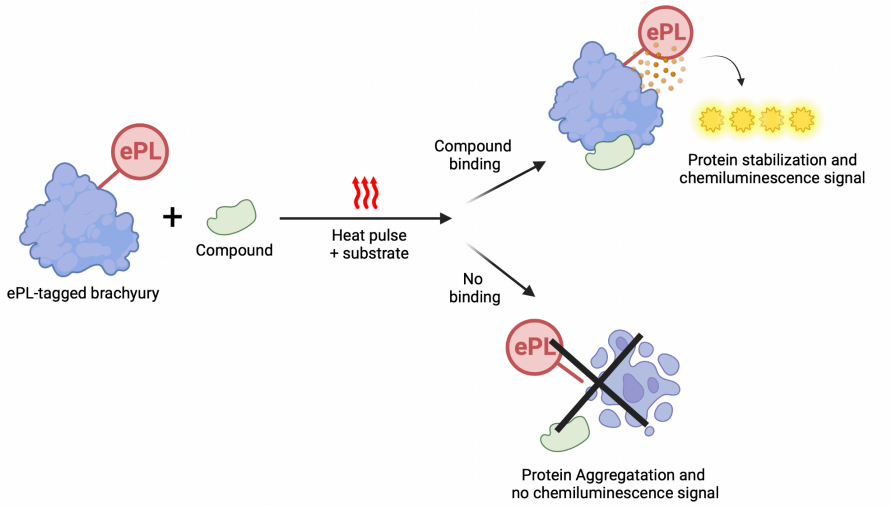

Fig. 5: Schematic of the InCELL Pulse Assay. Created with BioRender.com.

Transient transfection

The ePL tag was cloned on to the c-term of brachyury using the HiFi DNA Assembly Master mix (NEBuilder, New England Biolabs, USA). This was carried out by Dr. Hadley Sheppard prior the start of this master's project.

250,000 CH22 and U2OS cells were seeded on 6-well plates and allowed to adhere. CH22 cells were transfected with ePL tagged brachyury using the TransIT-LT1 Transfection Reagent (Mirus Bio LLC, USA) following manufacturer's instructions. For transfection of U2OS cells with ePL tagged brachyury, Lipofectamine 3000 Transfection Reagent (Thermo Fisher Scientific, USA) was used according to manufacturer's protocol. Both cell lines were incubated at 37 °C for 24 hours.

Identifying thermal denaturation temperature

To identify the thermal denaturation temperature for sensitive detection of target engagement, cells were exposed to a heat gradient in the presence or absence of brachyury inhibiting compounds. All Compounds were diluted with cell culture media to a final concentration of 20 µM, an equivalent concentration of DMSO served as control. Transfected cells were washed with 1X phosphate buffered saline (PBS) and trypsinized. Cell pellets were resuspended in diluted compounds or DMSO and 4000 cells/40 µl per well were seeded on a 96-well black PCR (Thermo Fisher Scientific, 0.2 ml Skirted 96-well PCR Plate). The covered plate was incubated

for 3 hours at 37 °C. Heat pulse was performed using a thermocycler (C1000 Touch Thermal Cycler, Bio-Rad Laboratories, USA) set at a temperature gradient of 40 - 55 °C for 3 minutes followed by cooling at 22 °C for 3 minutes. The lid temperature was set to 60 °C. 50 µl of detection solution (InCELL Detection Kit, DiscoveRX, USA) **(Tab. 9)** were added to each well directly afterwards. The plate was incubated covered for 1 hour at room temperature. Chemiluminescent signal was read on a plate reader at 0.5 to 1.0 seconds/well. Raw chemiluminescence values were plotted against temperatures using GraphPad Prims (v.9).

Tab. 9: InCELL detection solution.

Component	Volume per reaction
Lysis Buffer	10 µl
EA Reagent	10 µl
Substrate Reagent	40 µl

Isothermal inhibitor concentration-response testing

Once the thermal denaturation temperature was determined, the assay was repeated for the evaluation of concentration-response. To achieve this, 250,000 U2OS cells per well were seeded in 6-well plates and transfected the following day. Compounds were diluted with DMSO to a final concentration of 10 mM. 5 µl of DMSO and diluted compounds were added to a 384 well source plate (Echo Qualified 384LDV Microplate, Labcyte Inc., USA). Compounds from the source plate were diluted to 1, 5, 10, 15 and 20 µM and transferred to a 96-well black PCR plate (Thermo Fisher Scientific, 0.2 ml Skirted 96-well PCR Plate) using an acoustic liquid handler (ECHO 550 Acoustic Liquid Handler, Beckman Coulter, USA). Transfected U2OS Cells were washed with 1X PBS and trypsinized. 4000 cells in 40 µl cell culture media were added to each well containing the diluted compounds. The plate was incubated for 3 hours at 37 °C. Samples where heat pulsed at 55 °C for 3 minutes followed by cooling at 22 °C for 3 minutes. Lid temperature was set to 60 °C. 50 µl of detection solution **(Tab. 9)** were added to each well and incubated covered for 1 hour at room temperature on a rotator. Chemiluminescent signal was read on a plate reader at 0.5 to 1.0 seconds/well. Raw chemiluminescence values of each concentration were depicted on a bar chart using GraphPad Prism (v.9).

2.9. Endogenous CRISPR-Cas9 brachyury genome editing

Templates for homology directed repair (HDR) **(Tab. 10)** were ordered as linear DNA fragments (Merck & Co., USA). SgRNA (Tab. 10) was designed using CRISPOR(101) and ordered as synthetic RNAs at Synthego.

Electroporation

To form the sgRNA-Cas9 RNP complex, 1 µg of sgRNA was mixed with 1 µg Cas9 nuclease (Integrated DNA Technologies, Inc., USA) and incubated for 15-30 min at room temperature. Per reaction, 1 µl of 5 µM template was added to the sgRNA-Cas9 complex. For electroporation 250,000 CH22 cells per electroporation were resuspended in 10 µl buffer R (Thermo Fisher Scientific, USA) and added to the RNP complex. Electroporation conditions were 1400 V, 10 ms, 4 pulses using the Neon transfection system kit (Thermo Fisher Scientific, USA). Cells were allowed to recover for a few days before repeating electroporation under the same conditions.

PCR and sanger sequencing

To validate the gene editing efficacy, templates were PCR amplified and subsequently sanger sequenced. Therefore, genomic DNA of CH22 cells was collected (Wizard SV Genomic DNA Purification System, Promega, USA) following manufacturer's protocol. DNA concentrations were determined using the NanoDrop spectrophotometer. Samples were PCR amplified with Cys122ser_F and Cys122ser_Rev primers **(Tab. 10)** using the Phusion High Fidelity Master mix. Reagents were mixed as described in Tab. 7. A negative control containing water instead of DNA was carried. Amplification was performed according to the protocol in **Tab. 8** using a thermocycler. For gel electrophoresis, PCR samples and negative control were mixed 1:5 with purple gel loading dye. Subsequently 5 µl of negative control, samples and GeneRuler 1kb Plus DNA ladder were loaded on a 2 % agarose gel. For the gel, 1 g of agarose was dissolved in 50 ml of 1X TAE buffer and 5 µl SYBR Safe DNA Gel Stain were added. Gels were imaged with the ChemiDoc Imaging System. Amplified samples were purified and DNA concentration was again measured using the NanoDrop spectrophotometer. Purified PCR samples were sequenced using the sanger sequencing service provided by Source BioScience.

Tab. 10: Primers, sgRNA and HDR template used for Cys122Ser gene editing.

Name	Sequence	Manufacturer
Cys122Ser sgRNA 1	ggguggauguagacgcagcu	Synthego, USA
Cys122ser_F	TGAAGGTGAACGTGTCTGGCCTGG	Integrated DNA technologies, USA
Cys122ser_Rev	TCAAGCAGCGTCCCTTCCCACAA	
Cys122Ser template	GAAGTACGTGAACGGGGAATGGGTGCC GGGGGGCAAGCCGGAGCCGCAGGCGC CAAGCAGCGTCTACATCCACCCCGACTC GCCCAACTTCGGGGCCCACTGGATGAA GGCTCCCGTC	Merck & Co., USA

Single cell cloning

For single cell cloning, cells were diluted to 3 cells/ml and seeded on clear polystyrene microplates (Corning Clear 96-well Microplates, Thermo Fisher Scientific, USA). Single cell clones were allowed to grow and transferred to clear 24-well plates. Once the clones grew confluent, genomic DNA was collected. DNA of single cell clones was PCR amplified under the same conditions as described and sent to sanger sequencing.

2.10. Nano-Glo HiBiT Lytic Detection Assay

To quantify brachyury expression in chordoma cells, endogenous brachyury was HiBiT tagged in chordoma cells using CRISPR-Cas9 technology. The HiBiT system uses a small epitope peptide-tag (HiBiT) nano luciferase fragment that is designed to bind to a complementary large subunit (LgBiT) and activate its luminescent activity in the presence of substrate **(Fig. 6)**.

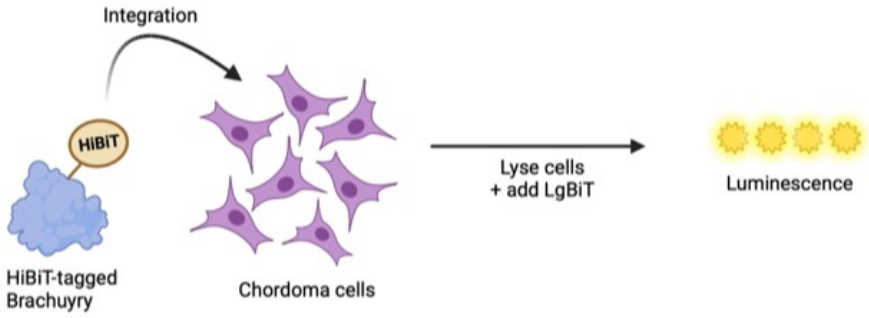

Fig. 6: Scheme of Nano-Glo HiBiT Lytic Detection Assay. Created with BioRender.com.

Endogenous brachyury tagging with HiBiT tag in UM-Chor1 cells

Endogenous tagging was performed by Dr. Hadley Sheppard using CRISPR-Cas9 technology. Therefore, templates for homology directed repair (HDR) were ordered as linear DNA fragments (Merck & Co., USA). SgRNA (sequence: tttcccgcgctctcggtgcc) was designed using CRISPOR(101) and ordered as synthetic RNAs at Synthego.

HiBiT assay

For validation of the editing, the cells were seeded in clear 24-well plates. After trypsinization the cells were transferred to small tubes and centrifuged at 1500 rpm for 5 minutes. The pellet was resuspended in 400 µl of cell culture media. Nano-Glo HiBiT Lytic Detection Assay (Promega, USA) and Cell-Titer Glo Luminescent Cell Viability Assay (Promega, USA) were performed in parallel with 100 µl of each sample seeded in a white 96-well polystyrene plate. Parental UM-Chor1 cells served as negative control and cell culture media was used as a blank. For the Nano-Glo HiBiT assay, 1:100 of LgBiT protein and 1:50 of HiBiT Lytic Substrate were mixed with HiBiT Lytic Buffer. 100 µl were added to each sample, mixed on a rocker for 1 minute and incubated for 20 minutes protected from light at room temperature. Cell-Titer Glo Luminescent Cell Viability Assay was accomplished as described in paragraph **2.6**. Luminescence signal was read with a plate reader (EnVision Multimode Plate Reader, PerkinElmer, USA). Individual luminescence values relative to the cell number were plotted on a bar chart using GraphPad Prism (v.9).

2.11. RT-qPCR

For reverse transcription quantitative real-time PCR (RT-qPCR), 250,000 CH22 cells per well were seeded on 6-well plates. The following day, cells were incubated for 7 hours with 10 µM of compound or DMSO diluted with cell culture media. RNA was collected using an RNA extraction kit (RNeasy Mini Kit, Qiagen, Germany). Concentration was measured using the NanoDrop spectrophotometer and all samples were diluted to a concentration of 800 ng/10µl. Total RNA was reverse transcribed to cDNA using the High-Capacity cDNA Reverse Transcription Kit (Thermo Fisher Scientific, USA) following the manufacturers protocol. cDNA was used for qPCR using the SYBR Green Master Mix (Thermo Fisher Scientific, USA) and uniquely designed gene expression probes (Integrated DNA technologies, USA) **(Tab. 11)**, including a *GAPDH* reference gene, in three technical replicates per reaction. The reaction mix was prepared according to Tab. 12 for the *T* and *GAPDH* transcript separately. Primers were diluted to a final concentration of 10 µM before adding them to the reaction mix. The reaction mix was transferred into a 384 well PCR plate. Samples were amplified using the ViiA 7 Real-Time PCR System (Applied Biosystems, USA).

Tab. 11: qPCR gene expression probes.

Name	Sequence	Manufacturer
t_qpcr-fwd	ATTTCCGTCCATTTCCCTCTC	Integrated DNA technologies, USA
t_qpcr-rev	ACCCAGGATCGTGGATCA	
GAPDH-Fwd	TGCACCACCAACTGCTTAGC	
GAPDH-Rev	GGCATGGACTGTGGTCATGAG	

Tab. 12: Reaction mix for qPCR.

Component	Volume per reaction
SYBR Green Master Mix	5 µl
Forward-Primer	0.5 µl
Reverse-Primer	0.5 µl
cDNA	1 µl
ddH_2O	3 µl
Total	10 µl

Analysis of RT-qPCR data

RT-qPCR data were analysed using the $\Delta\Delta C_T$ method. The ΔC_T values were calculated by subtraction of the average reference-gene (*GAPDH*) C_T values from average target-gene C_T values (three replicates each). $\Delta\Delta C_T$ values were calculated by subtracting ΔC_T values of the DMSO-treated from the ΔC_T of the compound-treated samples. The fold change in mRNA levels was calculated as $2^{-\Delta\Delta CT}$.

2.12. Fadraciclib xenograft study EXP2488

Handling of mice for the *in vivo* PK/PD study of fadraciclib was carried out by the animal facility at the ICR following the guidelines for the welfare and use of animals in cancer research (102). For this model, athymic nude mice were implanted subcutaneously with CH22 cells. Animals were matched by tumour volume and randomized to control and treatment groups. The mice were dosed at 40 mg/kg perorally daily for 4 days. Mice in the vehicle control group received water instead. Tumour and plasma samples were taken for pharmacokinetics/pharmacodynamics (PK/PD) analysis at 4 hours and 8 hours post last dose.

3. Results

3.1. Genotyping the chordoma-associated brachyury SNP

The purpose of this experiment was to investigate if the chordoma associated SNP (rs2305089) located at chr6:166579270 of the brachyury *T* gene is present in different chordoma cell lines in comparison to non-chordoma cell lines. To assess this, nine chordoma cell lines and two non-chordoma cell lines, SW420 and SW620, derived from an adenocarcinoma and express brachyury, were genotyped by Sanger sequencing. Prior to this, PCR of all cell lines was performed to amplify a 350 bp DNA sequence of the brachyury genome that covers the SNP. Before sending the PCR samples to Sanger sequencing, they were loaded onto an agarose gel to evaluate the presence of a specific 350 bp sequence in each sample. The gel confirmed that all samples contain the amplified sequence for subsequent Sanger sequencing **(Fig. 7)**.

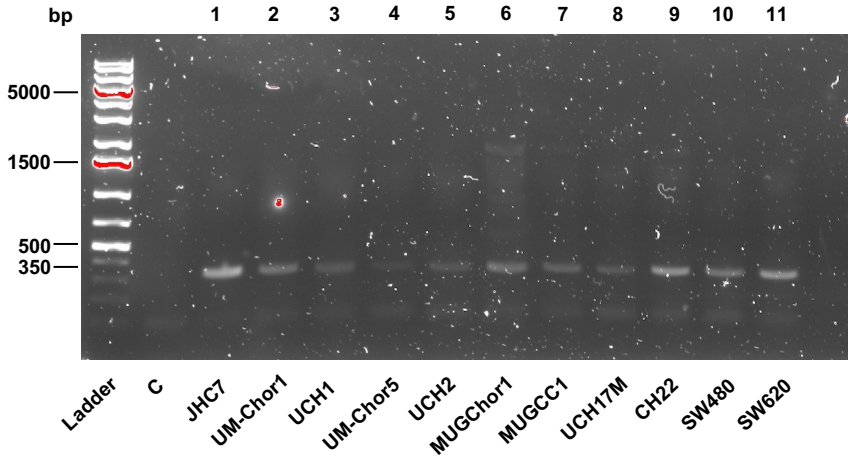

Fig. 7: The relevant sequence could be PCR amplified in all cell lines tested. 1 % agarose gel of PCR samples of 9 different chordoma cell lines (samples 1-9) and 2 non-chordoma cell lines (samples 10-11). ddH_2O served as negative control. The amplified sequence is 350 bp long.

The mutation that replaces a Guanin base by an Adenine was found in eight of the nine chordoma cell lines tested. Surprisingly, sequencing of the chordoma cell line CH22 did not show the replacement. As expected, both non-chordoma cell lines, SW480 and SW620, did not have the mutation as well. The next question was whether the mutation occurs in a homozygous or heterozygous form among the cell lines. From inspecting the trance of the Sanger sequencing data, it was noticeable that the SNP of most chordoma cell lines was homozygous. In UM-

Chor1 and UCH17M a heterozygous genotype was found **(Tab. 13)**. In summary, these results show that the chordoma associated SNP only occurs in chordoma cell lines and is mostly homozygously expressed. However, not all chordoma cell lines necessarily have this SNP. It is not present in brachyury of the non-chordoma cell lines tested.

Tab. 13: Genotyping of the chordoma-associated SNP (G177D).

Cell line	Chordoma/non-chordoma cell line	Genotype		Base pair
JHC7	Chordoma	homozygous	(-/-)	AA
UM-Chor1	Chordoma	heterozygous	(+/-)	GA
UCH1	Chordoma	homozygous	(-/-)	AA
UM-Chor5	Chordoma	homozygous	(-/-)	AA
UCH2	Chordoma	homozygous	(-/-)	AA
MUGChor1	Chordoma	homozygous	(-/-)	AA
MUGCC1	Chordoma	homozygous	(-/-)	AA
UCH17M	Chordoma	heterozygous	(+/-)	GA
CH22	Chordoma	homozygous	(+/+)	GG
SW480	Non-chordoma	homozygous	(+/+)	GG
SW620	Non-chordoma	homozygous	(+/+)	GG

3.2. Development of direct brachyury inhibitors

As part of the collaboration with the SGC, afatinib-derived brachyury inhibitors were developed and evaluated in cellular assays. Small molecules were made by the group of Dr. David Drewry at the UNC Chapel Hill, biophysical assays and crystallography were executed by the SGC at the University of Oxford.

3.2.1. Assessment of compound affinities to brachyury by mass spectrometry

During this master project, mass spectrometry analysis of 213 covalent compounds was performed in Oxford (103).

Tab. 14 lists the percentage labelling of brachyury protein after 60 minutes incubation at 5 µM of the top compounds.

Tab. 14: Percentage labelling of brachyury protein by mass spectrometry (60 minutes at 5 µM).

Compound	Percentage labelling
CF-8-69	100 %
CF-8-38	97 %
CF-8-70	87 %
CF-8-73	85 %
CF-8-137	81 %
CF-8-78	71 %
UNC-ZDG-173-1	51 %

As part of this work, the compounds with the highest percentage labelling were further assessed in a cell-based compound testing pipeline **(Fig. 8)**. Brachyury protein levels were analysed by western blotting. The compound's impact on cellular growth and correlating toxicity was investigated by performing a cell viability assay that measures the amount of ATP. The percentage of senescent cells was evaluated by a flow cytometry assay measuring

senescence-associated β-galactosidase (SA-β-gal) positive cells. Finally, target engagement in cells was examined by measuring protein stabilization correlating with compound binding.

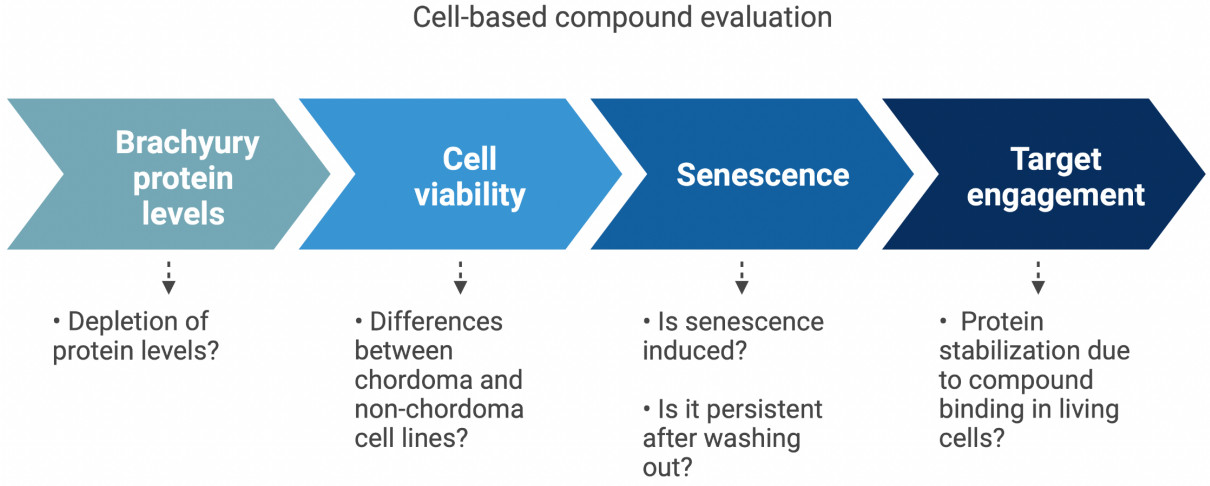

Fig. 8: Pipeline of afatinib-derived compound evaluation in cells.

3.2.2. Brachyury protein levels can be depleted by afatinib-derived compounds

To investigate the effect of compound treatment on brachyury protein levels in chordoma cells, CH22 cells were treated with each compound for 24 hours and a western blot was performed. It has been shown before in several chordoma cell lines, that treatment with the EGFR inhibitor afatinib downregulates brachyury (23). The depletion of brachyury protein levels in chordoma cells was again experimentally validated here. The western blot of afatinib shows a concentration dependent decrease of brachyury protein levels. Levels start to slightly decrease at 0.5 µM and significantly deplete at 5 µM, compared to the DMSO control **(Fig. 9)**.

Before the start of this master's project, quinazoline CF-8-38 and non-quinazoline UNC-ZDG-173-1 were considered as potent but amendable brachyury inhibitors. Since then, more analogues of these compounds were made and compared to the previous best ones to better understand how to improve their selectivity and potency for brachyury. The western blots of both CF-8-38 and UNC-ZDG-173-1 show depletion of brachyury protein levels at 1 µM and even greater reduction at 5 µM **(Fig. 9)**.

CF-8-69, CF-8-70, CF-8-78 and CF-8-137 analogues of CF-8-38 and UNC-ZDG-173-1 that all derive from afatinib. While CF-8-69, CF-8-70 and CF-8-78 are quinazolines, CF-8-137 is a

benzamide. Western blots of CF-8-69 and CF-8-70 show reduction of brachyury protein levels at 5 µM. CF-8-137 treatment leads to faint depletion of brachyury protein levels at 1 µM and more significantly at 5 µM. On the contrary, CF-8-78 and CF-8-73 do not deplete brachyury protein levels at concentrations less than or equal to 5 µM **(Fig. 9)**. In conclusion, afatinib is more potent at reducing brachyury protein levels in CH22 cells than the afatinib-derived compounds. Among the newest analogues, CF-8-137 depletes brachyury protein levels at the lowest concentration and the most significant.

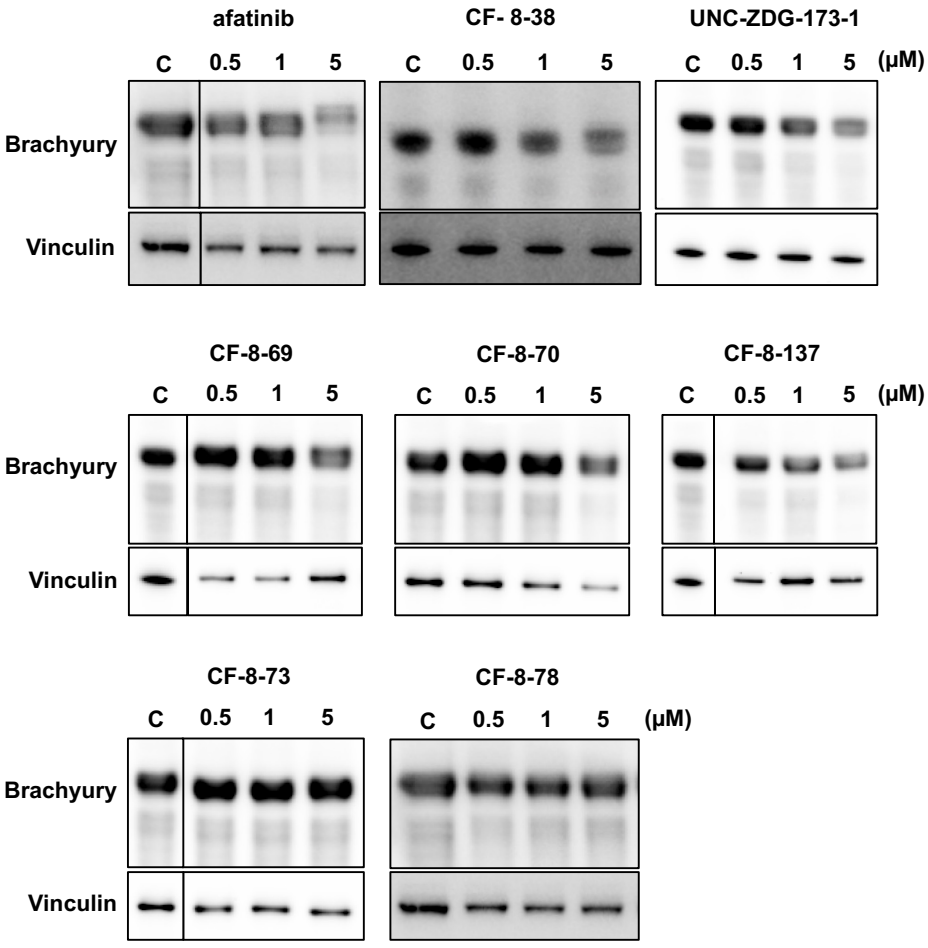

Fig. 9: Afatinib-derived compounds deplete brachyury protein levels. Western blot analysis of CH22 cells treated for 24 hours with the indicated concentrations of compound or DMSO as a control. Protein lysates were resolved on SDS-PAGE gel, transferred onto nitrocellulose membrane and probed with the indicated antibodies.

3.2.3. The new analogues have less impact on cell viability

To examine the effect on cellular growth of the compounds, a cell viability assay measuring the amount of ATP was performed. The assay was accomplished in both non-chordoma U2OS cells and CH22 chordoma cells to investigate selectivity for chordoma cells. The IC50 of afatinib in CH22 cells is 0.39 µM. The curves in **Fig. 10A** confirm that CH22 cells are more sensitive to afatinib than U2OS cells. Compared to other compounds, afatinib strongly induces growth inhibition of CH22 cells even at low concentrations.

The IC50 of CF-8-38 in CH22 cells is 1.2 µM and of UNC-ZDG-173-1 is 1.85 µM. The curves in **Fig. 10B-C** also indicate that CH22 cells are more sensitive to both compounds than the U2OS cells. CF-8-38 and UNC-ZDG-173-1 both inhibit cellular growth of CH22 cells relatively strongly compared to the new analogues.

CF-8-69 has an IC50 of 4.9 µM in CH22 cells. The curves of U2OS cells and CH22 cells show equal inhibition of cellular growth with this compound **(Fig. 10D)**. Compared to the previous best compounds and afatinib, it has lower impact on cell viability on chordoma cells.

CF-8-70 and CF-8-137 both have a relatively low impact on cell viability compared to afatinib and the previous best compounds UNC-ZDG-173-1 and CF-8-38. Cellular growth of CH22 cells is minimally more inhibited than U2OS cells **(Fig. 10E-F)**.

CF-8-73 shows only a minimal effect on cell growth of CH22 cells, while it does not affect U2OS cells at all **(Fig. 10G)**. The viability curves of CF-8-78 indicate that CH22 cells are more sensitive to the compound than U2OS cells **(Fig. 10H)**. Compared to the previous best compounds and afatinib, it has a lower impact on cell viability of chordoma cells.

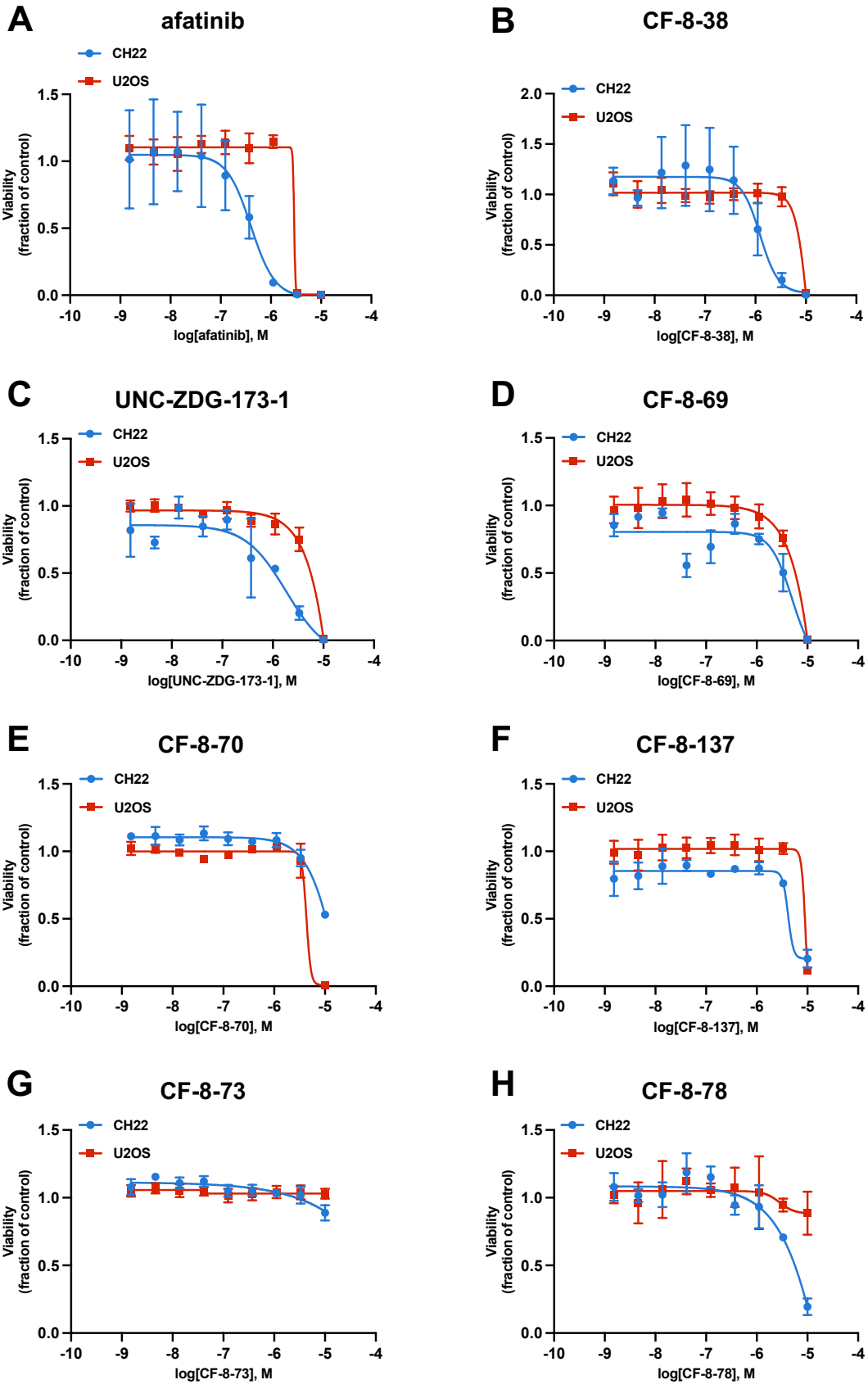
A
afatinib
CH22
U2OS
Viability (fraction of control)
log[afatinib], M
B
CF-8-38
log[CF-8-38], M
C
UNC-ZDG-173-1
log[UNC-ZDG-173-1], M
D
CF-8-69
log[CF-8-69], M
E
CF-8-70
log[CF-8-70], M
F
CF-8-137
log[CF-8-137], M
G
CF-8-73
log[CF-8-73], M
H
CF-8-78
log[CF-8-78], M

Fig. 10: Evaluation of cell viability. Response curves validating compound sensitivity in CH22 and U2OS cells. Cells were treated with the indicated concentration of compound and analysed for cell viability after 6 days. The X axis indicates the log of drug concentration and the Y axis shows viability relative to DMSO-treated cells (n=3 biological replicates). Error bars denote ± SD.

3.2.4. CF-8-70 and CF-8-137 induce senescence in chordoma cells

Senescence is the phenotypic outcome of selective brachyury inhibition (38). The hypothesis is that senescence inducing compounds are more likely act selective to brachyury than compounds that induce apoptosis. A senescence assay was performed to quantify the number of senescent cells after treating chordoma cells with covalent compounds.

Afatinib did not induce senescence in CH22 cells at 1 µM compared to the DMSO control **(Fig. 11A)**. It was not possible to perform the assay at a concentration of 5 µM afatinib, as most of the cells were apoptotic at this concentration, indicating a high toxicity. The graph of UNC-ZDG-173-1 shows 20 % senescent cells at 5 µM in comparison to 10 % for the control sample **(Fig. 11B)**. The newer analogue CF-8-78 shows a similar result **(Fig. 11E)**.

CF-8-69 and CF-8-73 did not induce senescence compared to the DMSO control **(Fig. 11C-D)**. CF-8-70 and CF-8-137 show the highest percentage of senescent cells, 50 % and 43 % respectively, compared to all other compounds tested **(Fig. 11F-G)**. The senescence phenotype was also microscopically observable after 6 days of treatment with both compounds (data not shown), resulting in a flat elongated cell morphology (38). To assess long-term effects of CF-8-70 and CF-8-137, cells were treated for 4 days and then compounds were removed for another 6 days. After washing out both compounds, cellular senescence remained **(Fig. 11H)**.

CF-8-38 did not participate in the quantification of senescent cells because of solubility issues we observed over time despite of the avoidance of multiple freezing and thawing of the compound. In summary, CF-8-70 and CF-8-137 significantly induced senescence in chordoma cells which was not rescued upon compound washout. This confirms that this is an irreversible phenotype.

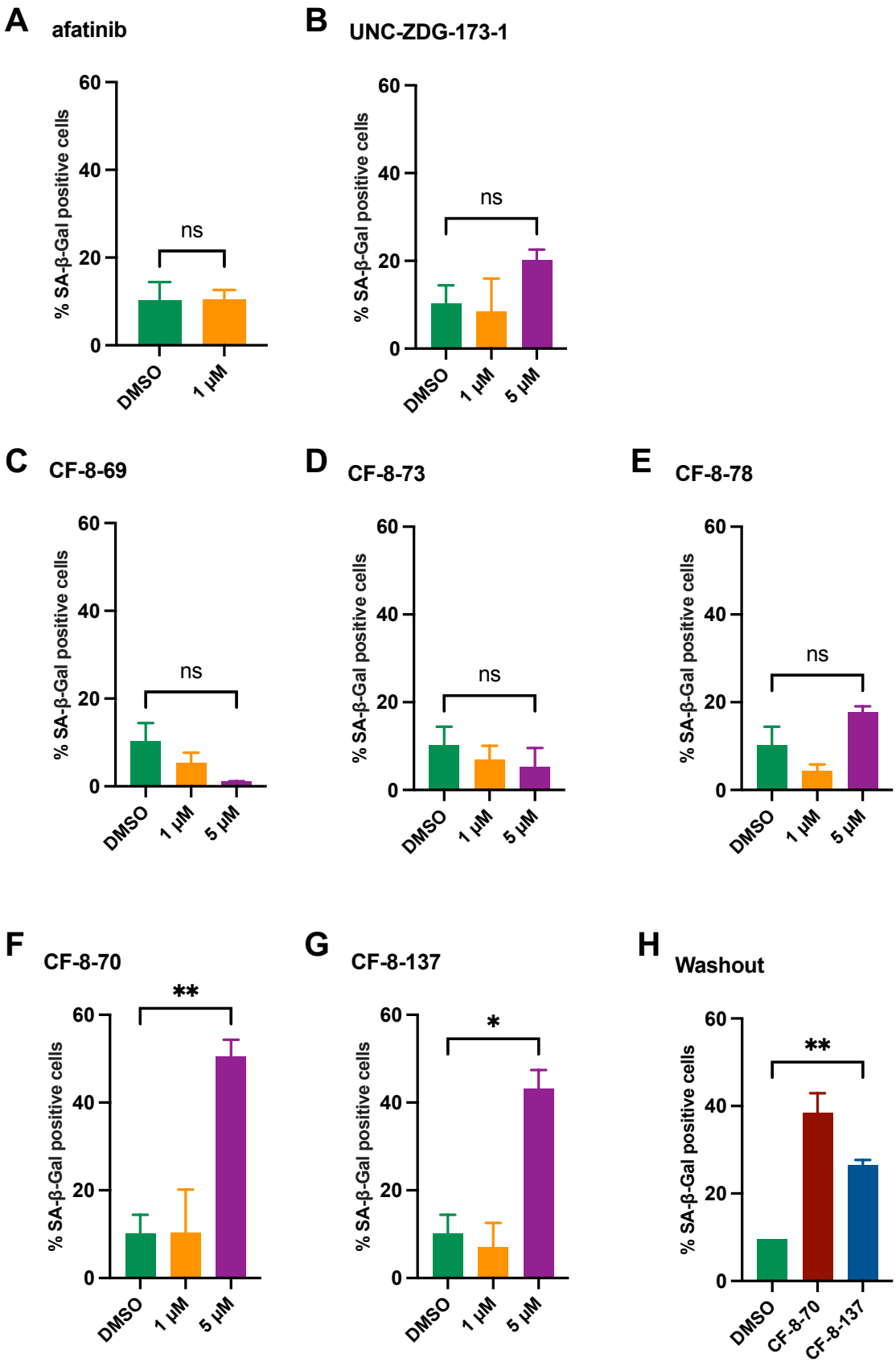
A
afatinib
% SA-β-Gal positive cells
60
40
20
0
ns
DMSO
1 μM
B
UNC-ZDG-173-1
% SA-β-Gal positive cells
60
40
20
0
ns
DMSO
1 μM
5 μM
C
CF-8-69
% SA-β-Gal positive cells
60
40
20
0
ns
DMSO
1 μM
5 μM
D
CF-8-73
% SA-β-Gal positive cells
60
40
20
0
ns
DMSO
1 μM
5 μM
E
CF-8-78
% SA-β-Gal positive cells
60
40
20
0
ns
DMSO
1 μM
5 μM
F
CF-8-70
% SA-β-Gal positive cells
60
40
20
0
**
DMSO
1 μM
5 μM
G
CF-8-137
% SA-β-Gal positive cells
60
40
20
0
*
DMSO
1 μM
5 μM
H
Washout
% SA-β-Gal positive cells
60
40
20
0
**
DMSO
CF-8-70
CF-8-137

Fig. 11: CF-8-70 and CF-8-137 induce senescence in CH22 cells. (A-G) Percentage of SA-β-gal positive CH22 cells treated with DMSO or the indicated concentration of the respective compound for 6 days. (H) Percentage of SA-β-gal positive CH22 cells treated with DMSO or 5 µM of CF-8-70 or CF-8-137 for 4 days, washed samples were analysed on day 10. Error bars denote ± SD (n=2 biological replicates). **P<0.01 and *P<0.05 derived from a two-tailed, unpaired *t*-test.

3.2.5. Afatinib shows concentration-dependent target engagement in U2OS cells

To measure compound binding to brachyury in a cellular environment, a target engagement assay was performed. First, the thermal denaturation temperature was determined by exposing cells to a heat gradient in the presence or absence of the compounds. For this, CH22 cells and U2OS cells were transiently transfected with ePL-tagged brachyury. In U2OS cells, protein stabilization through compound binding was achieved at around 52 °C with afatinib and to a lesser extent with CF-8-69. UNC-ZDG-173-1 showed no protein stabilization. **(Fig. 12A)**. No target engagement was obtained in CH22 cells **(Fig. 12B)**, which contain endogenous brachyury in addition to the transient ePL-tagged brachyury. Consequently, the subsequent concentration-response experiments were conducted in U2OS cells only.

At a short constant heat pulse of 55 °C, afatinib showed significant concentration-dependent protein stabilization **(Fig. 12C-D)**. For the covalent compound CF-8-69, a modest concentration-dependent stabilization was observed **(Fig. 12C)**. There was no significant protein stabilization in the remaining covalent compounds UNC-ZDG-173-1 **(Fig. 12C)**, CF-8-70 and CF-8-137 **(Fig. 12D)**, compared to the DMSO control.

Target engagement of the non-covalent compounds CF-8-169, UNC-AH-075D, CF-2-224 and UNC-AH-87B was tested under the same conditions as of the covalent compounds. None of these non-covalent compounds showed significant concentration-dependent target engagement **(Fig. 12E)**. In conclusion, we confirmed that the assay can be applied in U2OS cells which lack endogenous brachyury. Afatinib has proven to be an appropriate positive control for this assay. Except for CF-8-69, no concentration-dependent protein stabilization could be observed for the covalent and non-covalent compounds tested.

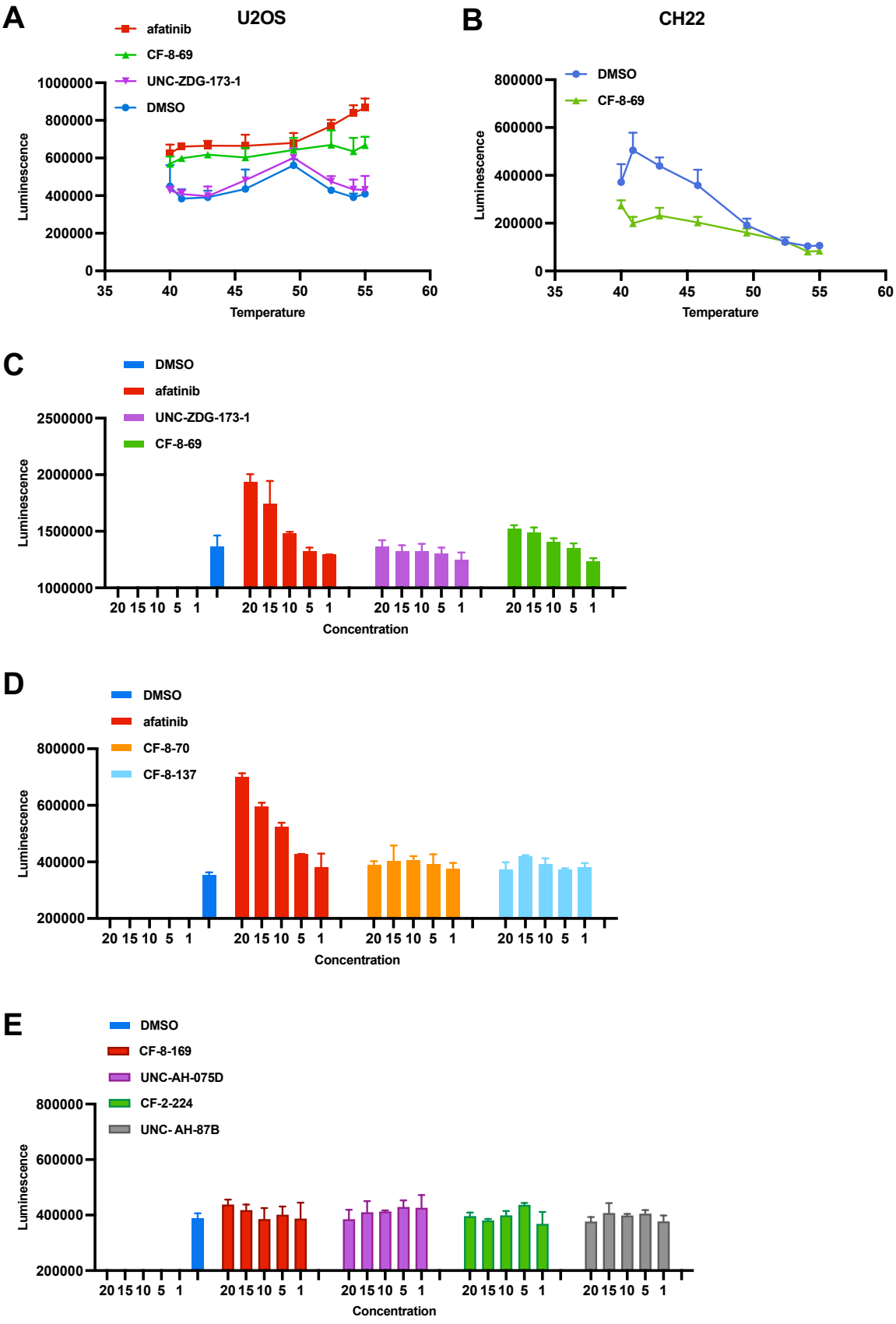
A
U2OS
afatinib
CF-8-69
UNC-ZDG-173-1
DMSO
Luminescence
Temperature
B
CH22
DMSO
CF-8-69
Luminescence
Temperature
C
DMSO
afatinib
UNC-ZDG-173-1
CF-8-69
Luminescence
Concentration
D
DMSO
afatinib
CF-8-70
CF-8-137
Luminescence
Concentration
E
DMSO
CF-8-169
UNC-AH-075D
CF-2-224
UNC- AH-87B
Luminescence
Concentration

Fig. 12: Target engagement assay of covalent and non-covalent compounds. (A) Target engagement (InCELL Pulse) assay of U2OS cells transfected with ePL-tagged brachyury. Cells were incubated for 3 hours with 20 µM of the indicated compound or DMSO as negative control. The X axis indicates the temperature of heat pulse and the Y axis shows the corresponding luminescence values. (B) Target engagement (InCELL Pulse) assay of CH22 cells transfected with ePL-tagged brachyury. Cells were incubated for 3 hours with 20 µM CF-8-69 or DMSO as negative control. The X axis indicates the temperature of heat pulse and the Y axis shows the corresponding luminescence values. (C-D) Target engagement (InCELL Pulse) assay of U2OS cells transfected with ePL-tagged brachyury. Cells were incubated for 3 hours with the indicated concentration of the respective compound or DMSO as negative control and heated at 55 °C. The X axis indicates the concentration in µM. The Y axis shows the corresponding luminescence values. Error bars denote ± SD (n=2 biological replicates).

3.2.6. Quantification of HiBiT-tagged brachyury in UM-Chor1 cells

Quantification of brachyury protein depletion after compound treatment is limited when performing western blots only. With the aim of having a more sensitive quantification method available for testing the compounds, HiBiT-tagged brachyury was integrated into UM-Chor1 cells using CRISPR-Cas9. This assay allows quantification of brachyury protein depletion after compound treatment directly in cell lysates. To determine whether the integration of HiBiT-tagged brachyury was successful, a HiBiT assay was performed in engineered clones and compared to parental UM-Chor1 cells. If the integration was successful, the expected luminescence signal of the respective clones would be much higher than the parental control. Looking at **Fig. 13**, it is apparent that the integration of HiBiT-tagged brachyury was not successful in the clones tested. The assay was accomplished in 40 clones total, clones numbered 30-40 (not depicted) showed similar results. Even if this attempt was not successful, it is worth repeating the integration as quantification with the HiBiT assay would provide useful results for compound evaluation.

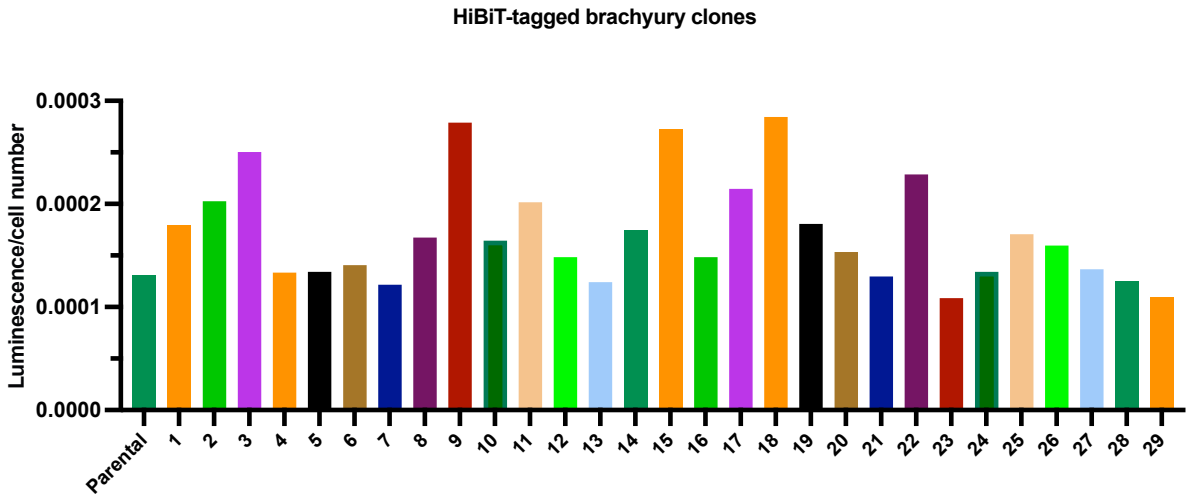

Fig. 13: Evaluation of HiBiT-tagged brachyury integration into UM-Chor1 cells. Bar graph depicting HiBiT luminescence values relative to cell number. Each number on the X axis (1-29) represents one clone.

3.2.7. Engineering of Cys122Ser clones

The covalent inhibitors which were developed in collaboration with the SGC bind to a specific cysteine residue of the brachyury protein located on exon 3. The purpose of this experiment was to allow further assessment of specific compound binding to brachyury in chordoma cells. To achieve this, the critical cysteine 122 was replaced by serine in CH22 chordoma cells using CRISPR-Cas9 technology **(Fig. 14)**. In total, 20 single cell clones were Sanger sequenced, resulting in one successfully edited clone. Cells of this serine clone can be used to evaluate whether the compounds are still able to bind to the altered brachyury, which would indicate unspecific binding.

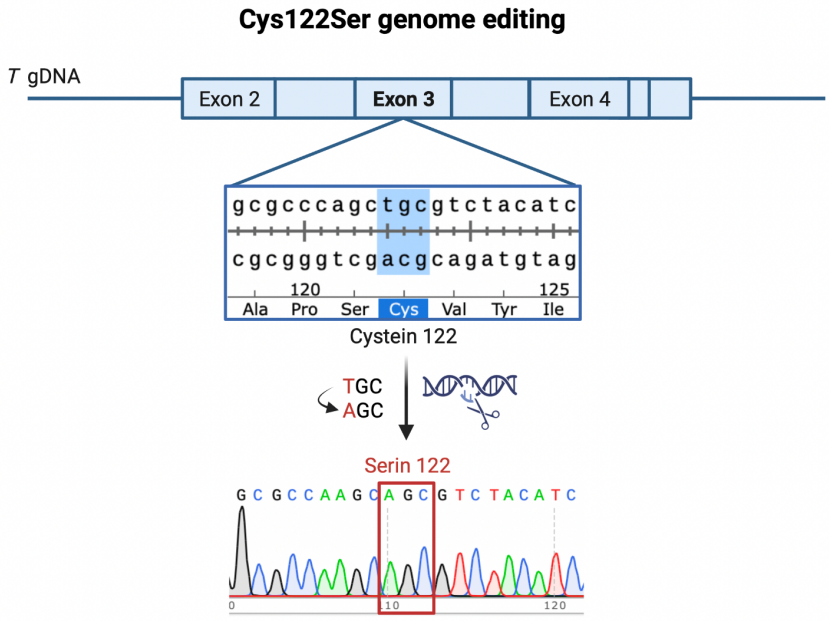

Fig. 14: Cys122Ser clone. CRISPR-Cas9 mediated single base pair editing of CH22 cells. Cystein 122 on exon 3 (blue) was changed to Serine 122 (red).

3.2.8. Analysis of *T* mRNA levels

In case of direct inhibition of the brachyury protein by the compounds, we assume that *T* mRNA levels of chordoma cells do not decrease in treated chordoma cells. To investigate how *T* mRNA levels are affected by compound treatment, RT-qPCR was performed after treating CH22 cells for 7 hours with afatinib, UNC-ZDG-173-1 and CF-8-38. Ct values of RT-qPCR replicates of *T* (gene of interest) and *GAPDH* (housekeeping gene) are illustrated in **Tab. 15**.

Tab. 15: Ct values of RT-qPCR replicates of *T* and *GAPDH* transcript.

	***T* Ct1**	***T* Ct2**	***T* Ct3**	***GAPDH* Ct1**	***GAPDH* Ct2**	***GAPDH* Ct3**
DMSO	19.42	19.37	20.23	15.04	15.15	15.00
afatinib	20.11	19.85	20.06	15.02	15.00	15.03
CF-38-8	20.91	20.86	20.86	15.08	15.08	15.05
UNC-ZDG-173-1	22.08	20.34	20.19	15.31	14.98	14.98

The $\Delta\Delta C_T$ method was used to analyse the difference between *T* and *GAPDH* expression **(Fig. 15A)**. All compounds induced depletion of mRNA levels in CH22 cells. Interestingly, afatinib treated cells showed less reduction of mRNA levels compared to UNC-ZDG-173-1 and CF-8-38 treatment. Reduction of *T* mRNA levels indicates that compound treatment also affects brachyury transcription. These results suggest that transcriptional alterations may contribute to the described brachyury depletion induced by these compounds. It needs to be considered, that in this investigation the standard deviation (SD) of Ct values of the *T* replicates for DMSO (SD = 0.48) and for UNC-ZDG-173-1 (SD = 1.05) treated cells are sources of error **(Fig. 15B)**.

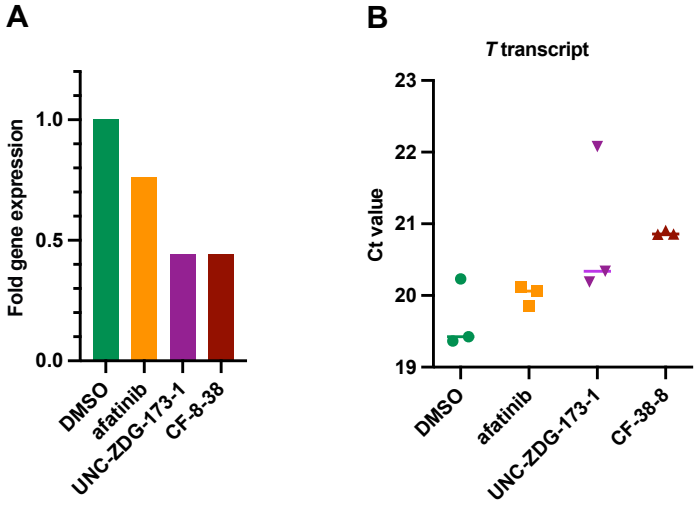

Fig. 15: Analysis of *T* mRNA levels. (A) Bar graph depicting fold change of *T* mRNA levels in CH22 cells treated with 10 µM of the indicated compound or DMSO as a control. Values were calculated using $\Delta\Delta C_T$ method. (B) Scatter showing Ct values of *T* transcript of CH22 cells treated with 10 µM of the indicated compound or DMSO as a control (n=3 biological replicates).

3.3. Targeting brachyury transcription with fadraciclib

In contrast to the ultimate development of novel direct brachyury inhibitors, clinical transcriptional CDK inhibitors represent a more immediate approach for the treatment of chordomas. The transcriptional CDK9/2 inhibitor fadraciclib (CYC065) was developed by the ICR and Cyclacel and is currently tested in phase 1/2 clinical trials in various solid tumours and leukemias. CDK2 is a key cell cycle regulator, promotes DNA replication and acts a part in DNA damage response (84), whereas CDK9 plays a role in transcriptional elongation (104). Fadraciclib has been shown to potently kill neuroblastoma cells through downregulation of MYCN, which is amplified in neuroblastoma cells and regulated by SEs (105). Given this, it was hypothesized that fadraciclib could downregulate brachyury and kill chordoma cells.

3.3.1. Fadraciclib: Approval of brachyury depletion and sensitivity

Previous work has already proven that fadraciclib downregulates brachyury and arrests growth of chordoma cells (unpublished). To confirm this, CH22 cells were treated with fadraciclib and a western blot was performed. Indeed, brachyury levels depleted at 0.5 µM **(Fig. 16A)**. Furthermore, treatment with fadraciclib in a serial dilution starting at 10 µM was able to completely arrest CH22 cell growth relative to controls **(Fig. 16B)**. This suggests that part of the growth arrest is due to brachyury downregulation.

The effect of fadraciclib on brachyury protein levels was further examined in UM-Chor1 chordoma cells additionally to CH22 cells. A time course with fadraciclib treatment shows depletion of brachyury protein levels in both cell lines after 24 hours **(Fig. 16C-D)**. Cleavage of PARP-1 by caspases is considered to be a hallmark of apoptotic cell death (106). Apoptosis was induced in both fadraciclib treated cell lines after 24 hours as shown by cleaved PARP. CDK9 plays a role in phosphorylation of serine 5 and serine 2 residues of RNA pol II, which is considered as a hallmark of productive elongation (107). Levels of phosphorylated Ser2 and Ser5 of RNA pol II were depleted in both chordoma cell lines **(Fig. 16C-D)**, which constitutes evidence for fadraciclib mediated CDK9 inhibition. Apart from that, Fadraciclib rapidly depleted MCL-1 protein, a biomarker for fadraciclib on-target activity (83,105). These findings indicate that both chordoma cell lines are sensitive to fadraciclib and that it can target brachyury.

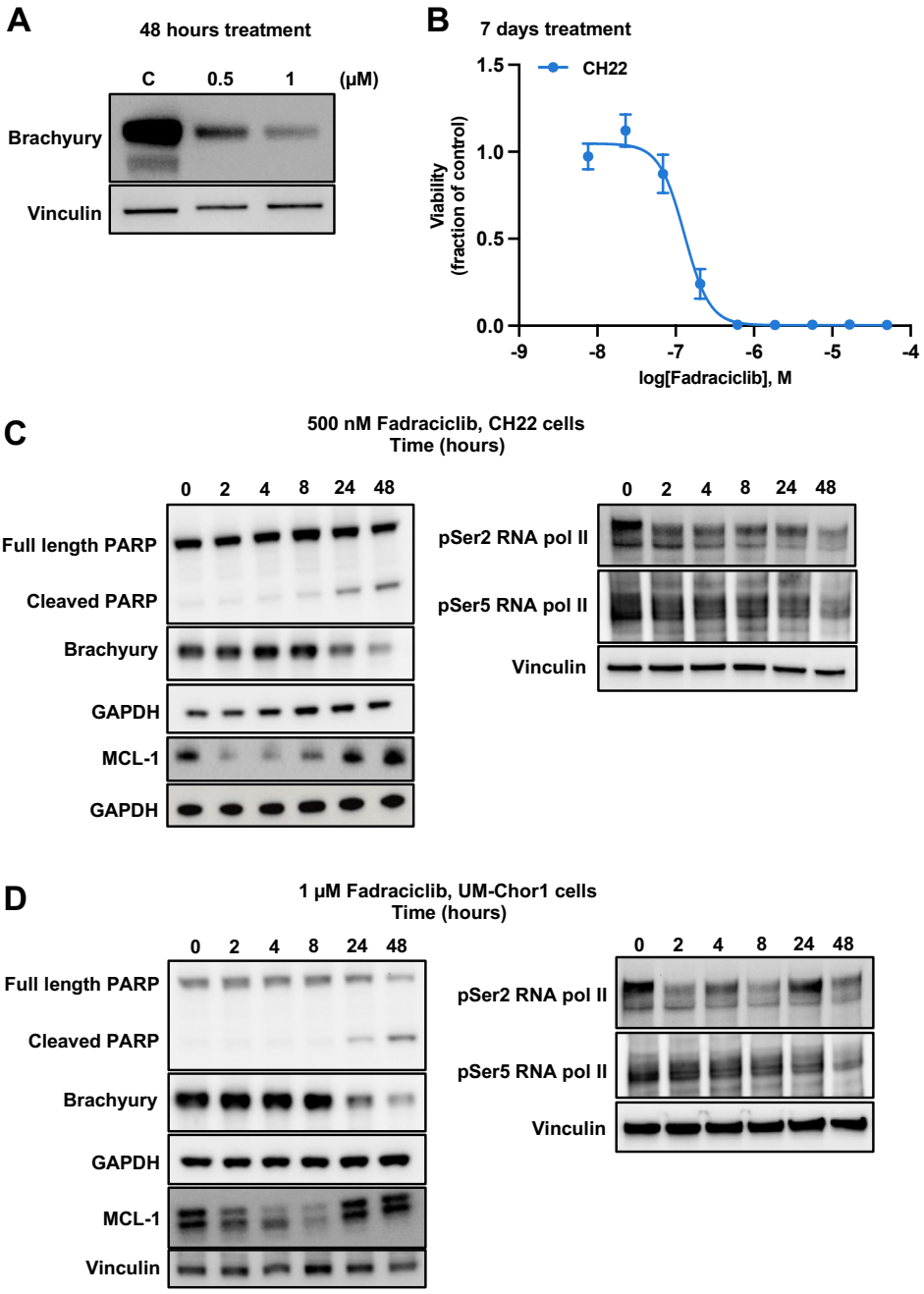

Fig. 16: Fadraciclib depletes brachyury levels as well as downstream targets and affects viability of chordoma cells. (A) Western blot analysis of CH22 cells treated for 48 hours with the indicated concentrations of fadraciclib or DMSO as a control. Protein lysates were resolved on SDS-PAGE gel, transferred onto nitrocellulose membrane and probed with the indicated antibodies. (B) Response curves validating fadraciclib sensitivity in CH22 cells. Cells were treated with the indicated concentration of compound and analysed for cell viability after 7 days. The X axis indicates the log of drug concentration and the Y axis shows response (cellular viability relative to DMSO-treated cells in three biological replicates). (C) Western blot analysis of CH22 cells treated with 500 nM fadraciclib for the indicated time (hours). Protein lysates were resolved on SDS-PAGE gel, transferred onto nitrocellulose membrane and probed with the indicated antibodies. (D) Western blot analysis of UM-CHor1 cells treated with 1 μM fadraciclib for the indicated time (hours). Protein lysates were resolved on SDS-PAGE gel, transferred onto nitrocellulose membrane and probed with the indicated antibodies.

3.3.2. Fadraciclib sensitizes chordoma cells for senolytic agents

Previous experiments have revealed that fadraciclib also induces a cellular senescence phenotype (unpublished). Although fadraciclib halts chordoma cell growth, the induction of senescence rather than cell killing raises concern that chordoma cells could eventually reengage their cell cycle and resume growth. Senolytic agents represent an attractive therapeutic strategy in combination with fadraciclib as they could selectively kill senescent cells. To assess if apoptosis can be induced in senescent chordoma cells that have been treated with fadraciclib, A-1331852 was added in combination. A-1331852 selectively inhibits BCL-xL (108), an anti-apoptotic protein that is upregulated in senescent cells (109).

For this experiment, CH22 cells were treated with 250 nM Fadraciclib for five days to achieve senescence before 1 µM or 5 µM of the BCL-xL inhibitor A-1331852 were added and incubated for another two days. For the fadraciclib-only control, cells were incubated with 250 nM of fadracilcib for eight days. Cells were treated with 1 µM or 5 µM of A-1331852 for the A-1331852-only control. The western blot in **Fig. 17A** shows an upregulation of cleaved PARP after fadraciclib treatment was combined with A-1331852. In comparison to this, treatment with only one of these compounds resulted in lower cleaved PARP levels. This was confirmed by quantification of the western blot band volumes **(Fig. 17B)**. What emerges from the results reported here is that the combination of fadraciclib with senolytic agents like A-1331852 can increase apoptosis associated proteins in chordoma cells.

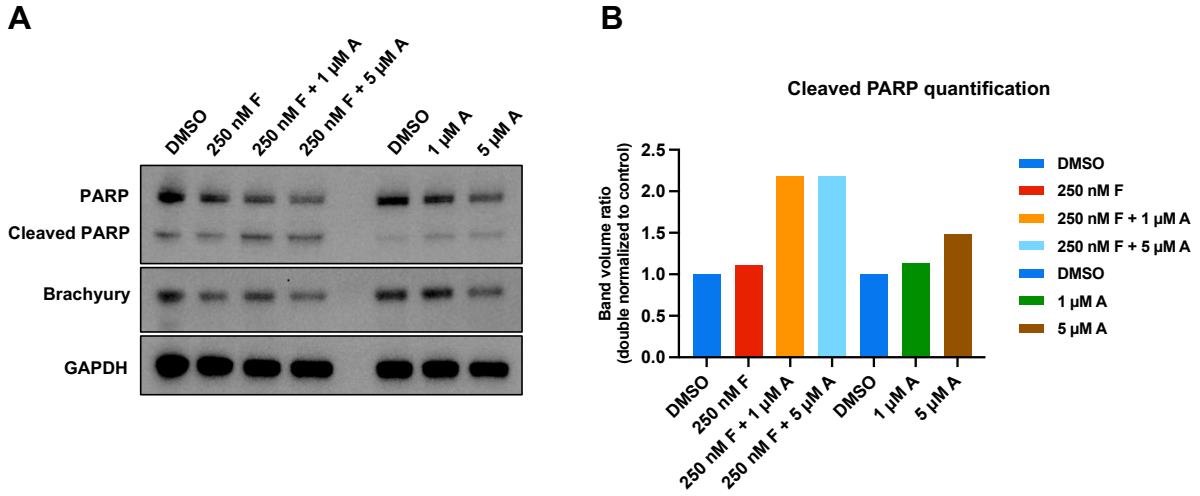

Fig. 17: Treatment of CH22 cells with Fadraciclib combined with A-1331852. (A) Western blot analysis of CH22 cells treated with the indicated concentrations of fadraciclib (indicated by “F”) and/or A-1331852 (indicated

by “A”) or DMSO as a control. A-1331852 was added on day 6 of fadraciclib treatment, cells were collected on day 8. Protein lysates were resolved on SDS-PAGE gel, transferred onto nitrocellulose membrane and probed with the indicated antibodies. (B) Quantification of cleaved PARP bands. Values were double normalized to GAPDH and DMSO control values.

3.3.3. Verification of the maximum tolerated dose of fadraciclib in a xenograft mouse model (EXP2488)

Two recent *in vivo* studies tested the effect of fadraciclib on brachyury in a paediatric patient derived xenograft (PDX) model in nude mice derived from a 11-year-old male patient with a metastatic clival chordoma tumour (unpublished). The first experiment (CF365) has revealed depletion of brachyury levels in tumour samples after a 3-day treatment with 50 mg/kg fadraciclib compared to the untreated control group. A second experiment (CF466) aimed to compare the efficacy of 50 mg/kg fadraciclib once a day (QD) and 25 mg/kg twice a day (BID) treatment in the same PDX model. Potent tumour growth inhibition was induced in the QD treatment group after 42 days of treatment. At the same time, severe tolerability issues occurred, which made it necessary to change the QD dosage to 40 mg/kg halfway through the study.

As a consequence of the described tolerability issues in the previous experimental set-up, a new maximum tolerable dose that still depletes brachyury levels was aimed to be reviewed. To achieve this, a CH22 xenograft nude mice model was treated with 40 mg/kg QD for 4 days **(Fig. 18A)**. The western blot of tumour samples shows no significant depletion of brachyury protein levels in the fadraciclib treated group, neither after 4 hours nor 8 hours post last dose. Also, MCL-1 protein, the biomarker of fadraciclib on-target activity, did not decrease in this group. Furthermore, target inhibition was not achieved as levels of phosphorylated Ser2 of RNA pol II did not deplete after treatment **(Fig. 18B)**. In conclusion, these results did not confirm the expected brachyury depleting effects of fadraciclib.

Pharmacokinetics analysis of EXP2488 revealed low plasma and tumour concentrations of fadraciclib. The total plasma and tumour concentrations of most samples were below the GI50 of 250 nM in CH22 cells and all free plasma concentrations were below the GI50 of 168 nM in CH22 cells **(Fig. 18C)**. Furthermore, total plasma concentration values were relatively low in comparison to previous studies in mouse model CF365 and CF466 **(Fig. 18D)**.

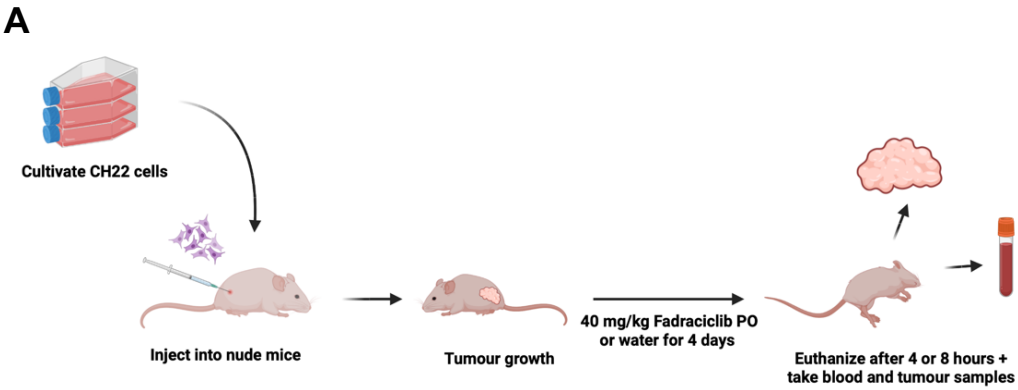

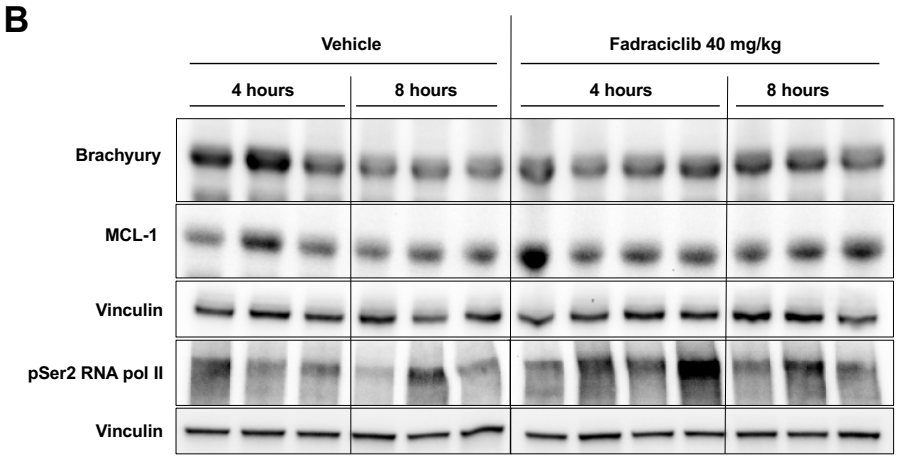

C

Fadraciclib concentration

Sample ID	Total plasma conc (nM)	Free plasma conc (nM)	Total tumour conc (nM)
A1 M1B1 Vehicle 4hrs	0.0	0.0	0
A2 M2B1 Vehicle 4hrs	0.0	0.0	0
A3 M3B1 Vehicle 4hrs	0.0	0.0	0
A4 M1B3 Vehicle 8hrs	0.0	0.0	0
A5 M2B3 Vehicle 8hrs	0.0	0.0	0
A6 M3B3 Vehicle 8hrs	0.0	0.0	0
A7 M1B2 CYC065 4hrs	102.7	4.5	39.2
A8 M2B2 CYC065 4hrs	162.8	7.1	N/A
A9 M3B2 CYC065 4hrs	95.7	4.2	N/A
A10 M4B2 CYC065 4hrs	269.3	11.8	171.4
A11 M1B4 CYC065 8hrs	6.6	0.3	4.9
A12 M2B4 CYC065 8hrs	9.6	0.4	10.2
A13 M3B4 CYC065 8hrs	55.6	2.4	30.9
A14 M4B4 CYC065 8hrs	16.0	0.7	9.8

D

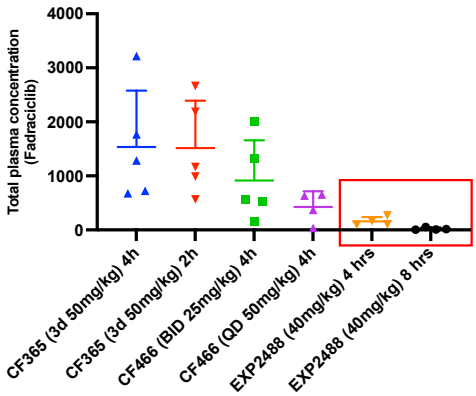

Fig. 18: Evaluation of protein levels of a fadraciclib treated xenograft mouse model (EXP2488). (A) Scheme of experimental set-up of EXP2488. Created with BioRender.com. (B) Western blot analysis of tumour samples from mice treated with either 40 mg/kg fadraciclib or water as a vehicle control. Tumours were collected after 4 hours or 8 hours post last dose. Protein lysates were resolved on SDS-PAGE gel, transferred onto nitrocellulose membrane and probed with the indicated antibodies. (C) Total plasma, free plasma and total tumour fadraciclib concentrations of treatment and control group. Plasma and tumours were collected after 4 hours or 8 hours post

last dose. (D) Comparison of total plasma fadraciclib concentrations of previous fadraciclib treated models (CF365, CF466) and last model (EXP2488).

4. Discussion

4.1. The chordoma associated SNP

The chordoma-associated brachyury SNP and its consequences have been a source of interest in the chordoma field for a long time. More than 90 % off all chordoma patients have the SNP (52) and it is known that it contributes to an increased risk of chordoma development (55). As part of this master thesis, the chordoma associated SNP was investigated by Sanger sequencing in different chordoma cell lines and brachyury expressing non-chordoma cell lines. The SNP was found in eight of nine chordoma cell lines and was not present in the non-chordoma cell lines tested. Furthermore, a homozygous AA genotype was found in six chordoma cell lines. These data consist with previous findings in European patient cohorts, showing that the SNP is present in a considerably high percentage and that the homozygous genotype is more frequent than the heterozygous genotype in chordomas (52,55).

4.1.1. RNA-Sequencing as further approach

Numerous transcription factors have been demonstrated to develop genetic aberrations leading to oncogene transformation, such as *MYCN* in neuroblastoma or fusion of *PAX3-FOXO1* (110) in rhabdomyosarcoma (111). These genetic aberrations cause an altered regulatory landscape that enables tumorigenesis. Keeping in mind that mutations within super enhancers can be critical within the context of the disease, it is important to further investigate the functional consequences of the chordoma associated SNP. The polymorphism is located within the DNA binding domain of brachyury and affects the binding ability of the transcription factor (53). From previous investigations it is known that the AA genotype correlates with higher *T* mRNA levels and enrichment of downstream targets (52). RNA sequencing (RNA-seq) represents a further approach to elucidate potential changes in gene expression associated with the SNP.

4.1.2. CH22 cells lack the SNP

It was surprising that CH22 cells do not have the G177D brachyury variant as the cell line was described heterozygous for the variant in previous studies (38). In the context of the evaluation of brachyury inhibitors, it might be useful to consider the genotyping of the SNP when selecting

the cell line. Further investigation of the functional consequences of the SNP in these cell lines could also be beneficial for compound development.

4.2. Developing direct brachyury inhibitors

Transcription factors have historically been considered undruggable, but this view recently shifted after the successful inhibition of transcription factors like *MYC* (112) or *STAT3* (113). Before the start of this master project, the collaborative team of the SGC, consisting of structural biologists, medicinal chemists and functional biologists started to develop brachyury inhibitors. In 2021, the afatinib-derived covalent inhibitors CF-8-38 and UNC-ZDG-173-1 were described we continued testing them in cell-based assays. Both can deplete brachyury protein levels in chordoma cells, but seem quite toxic due to apoptosis, which is not the phenotypic outcome of selective brachyury inhibition (38).

During the lifetime of this master project the collaborative team has designed several analogues of these inhibitors for further improvement of selectivity and potency for brachyury. Part of the efforts in this thesis was to evaluate the new compounds in a pipeline of cellular assays and compare them with afatinib, UNC-ZDG-173-1 and CF-8-38. The analogues were tested for 1) their effect on brachyury levels, 2) inducing senescence, 3) the effect on cellular growth in chordoma cells and non-chordoma cells and 4) target engagement in cells. According to the first three stages of the compound testing pipeline, the two most promising compounds CF-8-70 and CF-8-137 modulate brachyury, induce senescence, and are less toxic to chordoma cells. Furthermore, washout of CF-8-70 and CF-8-137 maintains cellular senescence, confirming that this is an irreversible phenotype.

4.2.1. Trouble shooting the InCell Pulse assay

The last step of the outlined compound testing pipeline was the InCeLL Pulse target engagement assay. In U2OS cells, concentration-dependent protein stabilization of exogenous brachyury was achieved with afatinib and modestly with CF-8-69. The assay did not show any measurable protein stabilization in CH22 cells, neither with afatinib nor with the compounds. This might occur due to interactions of endogenous brachyury with the compounds. Therefore, the InCELL Pulse assay is not appropriate for target engagement validation in chordoma cells. U2OS cells do not express endogenous brachyury which allows the measurement of protein

stabilization in a cellular setting, although not in a chordoma cell-specific environment. The reason for the lack of protein stabilization with nearly all covalent and non-covalent compounds in U2OS cell remains to be elucidated.

4.2.2. RT-qPCR of brachyury-bound target genes as further approach

T mRNA levels were analysed in CH22 cells treated with afatinib, UNC-ZDG-173-1 and CF-8-38. Previous data showed that selective brachyury degradation does not affect nascent mRNA levels of global genes (38). It was hypothesized that the brachyury inhibitors do not decrease *T* mRNA levels. Although, RT-qPCR revealed a reduction of *T* mRNA levels after treatment with both compounds and afatinib. Given that brachyury autoregulates through a transcriptional condensate, brachyury protein inhibition through the compounds may have negative feedback on *T* expression. Selective brachyury inhibition downregulates nascent transcription of super enhancer-associated brachyury-bound target genes like *KRT18* (38). Hence, it would be interesting to measure mRNA levels of these genes after treatment with the compounds. If the compounds lead to direct brachyury inhibition, mRNA levels of brachyury-bound targets genes should selectively decrease in contrast to genes that lack brachyury binding.

4.2.3. Investigation of compound selectivity with a Cys122Ser mutant

In conclusion, the new covalent compounds represent promising progress towards developing a potent and selective brachyury chemical probe. Moving forward, as these are covalent inhibitors that bind a specific cysteine residue on the brachyury protein, CH22 Cys122Ser mutants were engineered. These cells allow to determine the effect of compounds both on brachyury levels and senescence induction. As the cysteine is critical for compound binding to brachyury, the serine mutant should not deplete brachyury protein and the senescence phenotype should be rescued.

4.3. Evaluation of fadraciclib in the context of chordoma

It was recently demonstrated that the *T* gene is driven by a super enhancer and that this regulation confers sensitivity to inhibitors of transcriptional CDKs (24,38). To accelerate the clinical translation of transcriptional CDK inhibition in chordoma, a collaboration with companies and academic laboratories was initiated to evaluate this class of drugs. Contributing to the work of testing Cyclacel Pharmaceuticals' CDK9 and CDK2 inhibitor fadraciclib was part of this thesis. The sensitivity of chordoma cells to fadraciclib and depletion of brachyury protein levels in two different chordoma cell lines could be demonstrated.

4.3.1. Senolytic agents in combination with fadraciclib

Selective brachyury degradation induces senescence in chordoma cells rather than apoptosis (38) and this also occurs with fadraciclib treatment (unpublished). Senolytic agents like the BCL-xL inhibitor A-1331852 could selectively kill these senescent cells and prevents that they could eventually resume growth. In this thesis it was shown that the combination of fadraciclib and A-1331852 treatment leads to an increase of apoptosis associated protein levels. These data suggest that senolytic agents in combination with fadraciclib treatment represent a potentially effective therapeutic strategy to selectively kill chordoma cells.

4.3.2. Trouble shooting of *in vivo* study (EXP2488)

In addition, a PK/PD study in a CH22 xenograft mouse model was conducted to determine a new maximum tolerated dose of fadraciclib that can modulate brachyury. After toxicity problems occurred at 50 mg/kg in a previous study, the dose was now lowered to 40 mg/kg. During the four days of treatment, no signs of toxicity arose with the new dose, however no depletion of brachyury levels was achieved in the tumours of the treatment group. This was accompanied with surprisingly low plasma concentrations, even in the samples collected four hours after the last treatment. The bottom line is that the drug exposure was too low and target inhibition could not be achieved as no pSer2 RNA pol II reduction was observed. It does look like there is some unexpected variability in the PK from this experiment and here it is worth mentioning that previous experiments were conducted in a different facility using a PDX mouse model. At this point it is not clarified whether there was an issue with the experiment or target inhibition just cannot be achieved *in vivo* with the dose administered. A repetition of the PK/PD study can help to provide a clear answer as to whether a drug exposure in vivo leading to inhibition of pSer2 and suppression of brachyury can be achieved. When downregulation of brachyury is accomplished, a full efficacy study can follow to survey the effect on tumour growth.

4.3.3. Benefits and limitations

With the advent of numerous highly selective transcriptional inhibitors, some of which are already in clinical trials (83,114), it is crucial to understand both their benefits and limitations. Although, transcriptional CDK inhibition is one way to target brachyury autoregulation in chordoma, the global effects must be considered as sources of on-target toxicity (38). Since transcriptional CDKs are essential for transcription, most cell types are killed when they are knocked out (84). Because inhibitors like fadraciclib target multiple CDKs, there will be non-brachyury selective effects (38). Nevertheless, transcriptional CDK inhibition represents a therapeutic strategy that can be implemented immediately, while direct brachyury inhibitors are in development.

Bibliography

1. Virchow, R. Untersuchungen Ueber Die Entwicklung Des Schaedelgrundes. Berlin, Germany: Druck und Verlag von Georg Reamer; 1857.

2. Vujovic S, Henderson S, Presneau N, Odell E, Jacques TS, Tirabosco R, et al. Brachyury, a crucial regulator of notochordal development, is a novel biomarker for chordomas. J Pathol. 2006 Jun;209(2):157–65.

3. Stiller CA, Trama A, Serraino D, Rossi S, Navarro C, Chirlaque MD, et al. Descriptive epidemiology of sarcomas in Europe: report from the RARECARE project. Eur J Cancer Oxf Engl 1990. 2013 Feb;49(3):684–95.

4. Ulici V, Hart J. Chordoma: A Review and Differential Diagnosis. Arch Pathol Lab Med. 2021 Jul 28;146(3):386–95.

5. Bakker SH, Jacobs WCH, Pondaag W, Gelderblom H, Nout RA, Dijkstra PDS, et al. Chordoma: a systematic review of the epidemiology and clinical prognostic factors predicting progression-free and overall survival. Eur Spine J. 2018 Dec;27(12):3043–58.

6. Pillay N. The role of brachyury in the pathogenesis of chordoma. :259.

7. McMaster ML, Goldstein AM, Bromley CM, Ishibe N, Parry DM. Chordoma: incidence and survival patterns in the United States, 1973±1995. :11.

8. Whelan J, McTiernan A, Cooper N, Wong YK, Francis M, Vernon S, et al. Incidence and survival of malignant bone sarcomas in England 1979–2007. Int J Cancer. 2012;131(4):E508–17.

9. WANG K, WU Z, TIAN K, WANG L, HAO S, ZHANG L, et al. Familial chordoma: A case report and review of the literature. Oncol Lett. 2015 Nov;10(5):2937–40.

10. Yang XR, Ng D, Alcorta DA, Liebsch NJ, Sheridan E, Li S, et al. T (brachyury) gene duplication confers major susceptibility to familial chordoma. Nat Genet. 2009 Nov;41(11):1176–8.

11. Eds, W.C.o.T.E.B. World Health Organization classification of soft tissue and bone tumors. Vol. 5. Lyon, Frances: IARC Press; 2020.

12. Lee IJ, Lee RJ, Fahim DK. Prognostic Factors and Survival Outcome in Patients with Chordoma in the United States: A Population-Based Analysis. World Neurosurg. 2017 Aug;104:346–55.

13. Wasserman JK, Gravel D, Purgina B. Chordoma of the Head and Neck: A Review. Head Neck Pathol. 2018 Jun;12(2):261–8.

14. Yeter HG, Kosemehmetoglu K, Soylemezoglu F. Poorly differentiated chordoma: review of 53 cases. APMIS Acta Pathol Microbiol Immunol Scand. 2019 Sep;127(9):607–15.

15. Shih AR, Cote GM, Chebib I, Choy E, DeLaney T, Deshpande V, et al. Clinicopathologic characteristics of poorly differentiated chordoma. Mod Pathol Off J U S Can Acad Pathol Inc. 2018 Aug;31(8):1237–45.

16. Wedekind MF, Widemann BC, Cote G. Chordoma: Current status, problems, and future directions. Curr Probl Cancer. 2021 Aug;45(4):100771.

17. Hung YP, Diaz-Perez JA, Cote GM, Wejde J, Schwab JH, Nardi V, et al. Dedifferentiated Chordoma: Clinicopathologic and Molecular Characteristics With Integrative Analysis. Am J Surg Pathol. 2020 Sep;44(9):1213–23.

18. Batista KMP, Reyes KYA, Lopez FP, Pelaz AC, Vega IF, Pendás JLL, et al. Immunophenotypic features of dedifferentiated skull base chordoma: An insight into the intratumoural heterogeneity. Contemp Oncol Poznan Pol. 2017;21(4):267–73.

19. Heery CR. Chordoma: The Quest for Better Treatment Options. Oncol Ther. 2016;4(1):35–51.

20. Young VA, Curtis KM, Temple HT, Eismont FJ, DeLaney TF, Hornicek FJ. Characteristics and Patterns of Metastatic Disease from Chordoma. Sarcoma. 2015;2015:517657.

21. Hsieh PC, Xu R, Sciubba DM, McGirt MJ, Nelson C, Witham TF, et al. Long-term clinical outcomes following en bloc resections for sacral chordomas and chondrosarcomas: a series of twenty consecutive patients. Spine. 2009 Sep 15;34(20):2233–9.

22. Samson IR, Springfield DS, Suit HD, Mankin HJ. Operative treatment of sacrococcygeal chordoma. A review of twenty-one cases. J Bone Joint Surg Am. 1993 Oct;75(10):1476–84.

23. Magnaghi P, Salom B, Cozzi L, Amboldi N, Ballinari D, Tamborini E, et al. Afatinib Is a New Therapeutic Approach in Chordoma with a Unique Ability to Target EGFR and Brachyury. Mol Cancer Ther. 2018 Mar;17(3):603–13.

24. Sharifnia T, Wawer MJ, Chen T, Huang QY, Weir BA, Sizemore A, et al. Small-molecule targeting of brachyury transcription factor addiction in chordoma. Nat Med. 2019 Feb;25(2):292–300.

25. Korzh V, Grunwald D. Nadine Dobrovolskaïa-Zavadskaïa and the dawn of developmental genetics. BioEssays News Rev Mol Cell Dev Biol. 2001 Apr;23(4):365–71.

26. Faial T, Bernardo AS, Mendjan S, Diamanti E, Ortmann D, Gentsch GE, et al. Brachyury and SMAD signalling collaboratively orchestrate distinct mesoderm and endoderm gene regulatory networks in differentiating human embryonic stem cells. Dev Camb Engl. 2015 Jun 15;142(12):2121–35.

27. Stemple DL. Structure and function of the notochord: an essential organ for chordate development. Dev Camb Engl. 2005 Jun;132(11):2503–12.

28. Naiche LA, Harrelson Z, Kelly RG, Papaioannou VE. T-box genes in vertebrate development. Annu Rev Genet. 2005;39:219–39.

29. Wilkinson DG, Bhatt S, Herrmann BG. Expression pattern of the mouse T gene and its role in mesoderm formation. Nature. 1990 Feb 15;343(6259):657–9.

30. Miettinen M, Wang Z, Lasota J, Heery C, Schlom J, Palena C. NUCLEAR BRACHYURY EXPRESSION IS CONSISTENT IN CHORDOMA, COMMON IN GERM CELL TUMORS AND SMALL CELL CARCINOMAS AND RARE IN OTHER CARCINOMAS AND SARCOMAS. AN IMMUNOHISTOCHEMICAL STUDY OF 5229 CASES. Am J Surg Pathol. 2015 Oct;39(10):1305–12.

31. Wilson V, Manson L, Skarnes WC, Beddington RS. The T gene is necessary for normal mesodermal morphogenetic cell movements during gastrulation. Dev Camb Engl. 1995 Mar;121(3):877–86.

32. Edwards YH, Putt W, Lekoape KM, Stott D, Fox M, Hopkinson DA, et al. The human homolog T of the mouse T(Brachyury) gene; gene structure, cDNA sequence, and assignment to chromosome 6q27. Genome Res. 1996 Mar;6(3):226–33.

33. Müller CW, Herrmann BG. Crystallographic structure of the T domain-DNA complex of the Brachyury transcription factor. Nature. 1997 Oct 23;389(6653):884–8.

34. Bank RPD. RCSB PDB - 6F58: Crystal structure of human Brachyury (T) in complex with DNA [Internet]. [cited 2022 Nov 23]. Available from: https://www.rcsb.org/structure/6f58

35. Kispert A, Koschorz B, Herrmann BG. The T protein encoded by Brachyury is a tissue-specific transcription factor. EMBO J. 1995 Oct 2;14(19):4763–72.

36. Herzog VA, Reichholf B, Neumann T, Rescheneder P, Bhat P, Burkard TR, et al. Thiol-linked alkylation of RNA to assess expression dynamics. Nat Methods. 2017 Dec;14(12):1198–204.

37. Pe W, Hj D. Intrinsically disordered proteins in cellular signalling and regulation. Nat Rev Mol Cell Biol [Internet]. 2015 Jan [cited 2022 Nov 23];16(1). Available from: https://pubmed.ncbi.nlm.nih.gov/25531225/

38. Sheppard HE, Dall'Agnese A, Park WD, Shamim MH, Dubrulle J, Johnson HL, et al. Targeted brachyury degradation disrupts a highly specific autoregulatory program controlling chordoma cell identity. Cell Rep Med. 2021 Jan;2(1):100188.

39. Presneau N, Shalaby A, Ye H, Pillay N, Halai D, Idowu B, et al. Role of the transcription factor T (brachyury) in the pathogenesis of sporadic chordoma: a genetic and functional-based study. J Pathol. 2011 Feb;223(3):327–35.

40. Roselli M, Fernando RI, Guadagni F, Spila A, Alessandroni J, Palmirotta R, et al. Brachyury, a driver of the epithelial-mesenchymal transition, is overexpressed in human lung tumors: an opportunity for novel interventions against lung cancer. Clin Cancer Res Off J Am Assoc Cancer Res. 2012 Jul 15;18(14):3868–79.

41. Fernando RI, Litzinger M, Trono P, Hamilton DH, Schlom J, Palena C. The T-box transcription factor Brachyury promotes epithelial-mesenchymal transition in human tumor cells. J Clin Invest. 2010 Feb;120(2):533–44.

42. Palena C, Roselli M, Litzinger MT, Ferroni P, Costarelli L, Spila A, et al. Overexpression of the EMT driver brachyury in breast carcinomas: association with poor prognosis. J Natl Cancer Inst. 2014 May 9;106(5):dju054.

43. Yamaguchi T, Suzuki S, Ishiiwa H, Ueda Y. Intraosseous benign notochordal cell tumours: overlooked precursors of classic chordomas? Histopathology. 2004 Jun;44(6):597–602.

44. Passamaneck YJ, Katikala L, Perrone L, Dunn MP, Oda-Ishii I, Di Gregorio A. Direct activation of a notochord cis-regulatory module by Brachyury and FoxA in the ascidian Ciona intestinalis. Dev Camb Engl. 2009 Nov;136(21):3679–89.

45. Yamaguchi T, Watanabe-Ishiiwa H, Suzuki S, Igarashi Y, Ueda Y. Incipient chordoma: a report of two cases of early-stage chordoma arising from benign notochordal cell tumors. Mod Pathol Off J U S Can Acad Pathol Inc. 2005 Jul;18(7):1005–10.

46. Choi KS, Harfe BD. Hedgehog signaling is required for formation of the notochord sheath and patterning of nuclei pulposi within the intervertebral discs. Proc Natl Acad Sci U S A. 2011 Jun 7;108(23):9484–9.

47. Barresi V, Ieni A, Branca G, Tuccari G. Brachyury: a diagnostic marker for the differential diagnosis of chordoma and hemangioblastoma versus neoplastic histological mimickers. Dis Markers. 2014;2014:514753.

48. McCarroll SA, Altshuler DM. Copy-number variation and association studies of human disease. Nat Genet. 2007 Jul;39(7 Suppl):S37-42.

49. Abe K, Kitago M, Kitagawa Y, Hirasawa A. Hereditary pancreatic cancer. Int J Clin Oncol. 2021;26(10):1784–92.

50. Yang X, Leslie G, Doroszuk A, Schneider S, Allen J, Decker B, et al. Cancer Risks Associated With Germline PALB2 Pathogenic Variants: An International Study of 524 Families. J Clin Oncol Off J Am Soc Clin Oncol. 2020 Mar 1;38(7):674–85.

51. Kelley MJ, Shi J, Ballew B, Hyland PL, Li WQ, Rotunno M, et al. Characterization of T gene sequence variants and germline duplications in familial and sporadic chordoma. Hum Genet. 2014 Oct;133(10):1289–97.

52. Pillay N, Plagnol V, Tarpey PS, Lobo SB, Presneau N, Szuhai K, et al. A common single-nucleotide variant in T is strongly associated with chordoma. Nat Genet. 2012 Nov;44(11):1185–7.

53. Papapetrou C, Edwards YH, Sowden JC. The T transcription factor functions as a dimer and exhibits a common human polymorphism Gly-177-Asp in the conserved DNA-binding domain. FEBS Lett. 1997 Jun 9;409(2):201–6.

54. Wu Z, Wang K, Wang L, Feng J, Hao S, Tian K, et al. The brachyury Gly177Asp SNP is not associated with a risk of skull base chordoma in the Chinese population. Int J Mol Sci. 2013 Oct 25;14(11):21258–65.

55. Jalessi M, Gholami MS, Razmara E, Hassanzadeh S, Sadeghipour A, Jahanbakhshi A, et al. Association between TBXT rs2305089 polymorphism and chordoma in Iranian patients identified by a developed T-ARMS-PCR assay. J Clin Lab Anal. 2022 Jan;36(1):e24150.

56. Kim TK, Shiekhattar R. Architectural and Functional Commonalities between Enhancers and Promoters. Cell. 2015 Aug 27;162(5):948–59.

57. Tang F, Yang Z, Tan Y, Li Y. Super-enhancer function and its application in cancer targeted therapy. Npj Precis Oncol. 2020 Feb 12;4(1):1–7.

58. Whyte WA, Orlando DA, Hnisz D, Abraham BJ, Lin CY, Kagey MH, et al. Master transcription factors and mediator establish super-enhancers at key cell identity genes. Cell. 2013 Apr 11;153(2):307–19.

59. Chipumuro E, Marco E, Christensen CL, Kwiatkowski N, Zhang T, Hatheway CM, et al. CDK7 inhibition suppresses super-enhancer-linked oncogenic transcription in MYCN-driven cancer. Cell. 2014 Nov 20;159(5):1126–39.

60. Lovén J, Hoke HA, Lin CY, Lau A, Orlando DA, Vakoc CR, et al. Selective inhibition of tumor oncogenes by disruption of super-enhancers. Cell. 2013 Apr 11;153(2):320–34.

61. Hnisz D, Abraham BJ, Lee TI, Lau A, Saint-André V, Sigova AA, et al. Super-enhancers in the control of cell identity and disease. Cell. 2013 Nov 7;155(4):934–47.

62. Darnell JE. Transcription factors as targets for cancer therapy. Nat Rev Cancer. 2002 Oct;2(10):740–9.

63. Look AT. Oncogenic transcription factors in the human acute leukemias. Science. 1997 Nov 7;278(5340):1059–64.

64. Dang CV, Reddy EP, Shokat KM, Soucek L. Drugging the 'undruggable' cancer targets. Nat Rev Cancer. 2017 Aug;17(8):502–8.

65. Arkin MR, Tang Y, Wells JA. Small-molecule inhibitors of protein-protein interactions: progressing toward the reality. Chem Biol. 2014 Sep 18;21(9):1102–14.

66. Jh B. Targeting transcription factors in cancer - from undruggable to reality. Nat Rev Cancer [Internet]. 2019 Nov [cited 2022 Nov 10];19(11). Available from: https://pubmed.ncbi.nlm.nih.gov/31511663/

67. Krönke J, Udeshi ND, Narla A, Grauman P, Hurst SN, McConkey M, et al. Lenalidomide causes selective degradation of IKZF1 and IKZF3 in multiple myeloma cells. Science. 2014 Jan 17;343(6168):301–5.

68. Mehta RS, Barlow WE, Albain KS, Vandenberg TA, Dakhil SR, Tirumali NR, et al. Combination anastrozole and fulvestrant in metastatic breast cancer. N Engl J Med. 2012 Aug 2;367(5):435–44.

69. Li X, Song Y. Proteolysis-targeting chimera (PROTAC) for targeted protein degradation and cancer therapy. J Hematol OncolJ Hematol Oncol. 2020 May 13;13(1):50.

70. Brachyury (TBXT) ligands for chordoma: 1. Fragment optimization strategy 2. fragment F9000505, B-site, PDB 5QRU – openlabnotebooks.org [Internet]. [cited 2022 Dec 3]. Available from: https://openlabnotebooks.org/brachyury-tbxt-ligands-for-chordoma-1-fragment-optimization-strategy-2-fragment-f9000505-b-site-pdb-5qru/

71. Deeks ED, Keating GM. Afatinib in advanced NSCLC: a profile of its use. Drugs Ther Perspect Ration Drug Sel Use. 2018;34(3):89–98.

72. EMA. Giotrif [Internet]. European Medicines Agency. 2018 [cited 2022 Dec 3]. Available from: https://www.ema.europa.eu/en/medicines/human/EPAR/giotrif

73. Bank RPD. RCSB PDB - 6ZU8: Crystal structure of human Brachyury G177D variant in complex with Afatinib [Internet]. [cited 2022 Dec 1]. Available from: https://www.rcsb.org/structure/6zu8

74. Nguyen HH, Park J, Kang S, Kim M. Surface plasmon resonance: a versatile technique for biosensor applications. Sensors. 2015 May 5;15(5):10481–510.

75. PubChem. Afatinib [Internet]. [cited 2022 Dec 3]. Available from: https://pubchem.ncbi.nlm.nih.gov/compound/10184653

76. Delmore JE, Issa GC, Lemieux ME, Rahl PB, Shi J, Jacobs HM, et al. BET bromodomain inhibition as a therapeutic strategy to target c-Myc. Cell. 2011 Sep 16;146(6):904–17.

77. Kwiatkowski N, Zhang T, Rahl PB, Abraham BJ, Reddy J, Ficarro SB, et al. Targeting transcription regulation in cancer with a covalent CDK7 inhibitor. Nature. 2014 Jul 31;511(7511):616–20.

78. Lasko LM, Jakob CG, Edalji RP, Qiu W, Montgomery D, Digiammarino EL, et al. Discovery of a selective catalytic p300/CBP inhibitor that targets lineage-specific tumours. Nature. 2017 Oct 5;550(7674):128–32.

79. Iwamoto M, Friedman EJ, Sandhu P, Agrawal NGB, Rubin EH, Wagner JA. Clinical pharmacology profile of vorinostat, a histone deacetylase inhibitor. Cancer Chemother Pharmacol. 2013 Sep;72(3):493–508.

80. Sumransub N, Murugan P, Marette S, Clohisy DR, Skubitz KM. Multiple malignant tumors in a patient with familial chordoma, a case report. BMC Med Genomics. 2021 Aug 31;14(1):213.

81. Cyclacel Pharmaceuticals, Inc. A Phase 1/2, Open-label, Multicenter Study to Investigate the Safety, Pharmacokinetics, and Efficacy of Fadraciclib (CYC065), an Oral CDK 2/9 Inhibitor, in Subjects With Advanced Solid Tumors and Lymphoma [Internet]. clinicaltrials.gov; 2022 Apr [cited 2022 Nov 29]. Report No.: NCT04983810. Available from: https://clinicaltrials.gov/ct2/show/NCT04983810

82. Cyclacel Pharmaceuticals, Inc. A Phase 1/2, Open Label, Multicenter Study to Investigate the Safety and Efficacy of Fadraciclib (CYC065), an Oral CDK 2/9 Inhibitor, in Subjects With Leukemias or Myelodysplastic Syndrome (MDS) [Internet]. clinicaltrials.gov; 2022 Apr [cited 2022 Nov 29]. Report No.: NCT05168904. Available from: https://clinicaltrials.gov/ct2/show/NCT05168904

83. Frame S, Saladino C, MacKay C, Atrash B, Sheldrake P, McDonald E, et al. Fadraciclib (CYC065), a novel CDK inhibitor, targets key pro-survival and oncogenic pathways in cancer. Lampe JN, editor. PLOS ONE. 2020 Jul 9;15(7):e0234103.

84. Lim S, Kaldis P. Cdks, cyclins and CKIs: roles beyond cell cycle regulation. Dev Camb Engl. 2013 Aug;140(15):3079–93.

85. Bačević K, Lossaint G, Achour TN, Georget V, Fisher D, Dulić V. Cdk2 strengthens the intra-S checkpoint and counteracts cell cycle exit induced by DNA damage. Sci Rep. 2017 Oct 18;7(1):13429.

86. Mandal R, Becker S, Strebhardt K. Targeting CDK9 for Anti-Cancer Therapeutics. Cancers. 2021 May 1;13(9):2181.

87. Jäger D, Lechel A, Tharehalli U, Seeling C, Möller P, Barth TFE, et al. U-CH17P, -M and -S, a new cell culture system for tumor diversity and progression in chordoma. Int J Cancer. 2018 Apr 1;142(7):1369–78.

88. Shah SR, David JM, Tippens ND, Mohyeldin A, Martinez-Gutierrez JC, Ganaha S, et al. Brachyury-YAP Regulatory Axis Drives Stemness and Growth in Cancer. Cell Rep. 2017 Oct 10;21(2):495–507.

89. Liu X, Nielsen GP, Rosenberg AE, Waterman PR, Yang W, Choy E, et al. Establishment and characterization of a novel chordoma cell line: CH22. J Orthop Res Off Publ Orthop Res Soc. 2012 Oct;30(10):1666–73.

90. Scheil S, Brüderlein S, Liehr T, Starke H, Herms J, Schulte M, et al. Genome-wide analysis of sixteen chordomas by comparative genomic hybridization and cytogenetics of the first human chordoma cell line, U-CH1. Genes Chromosomes Cancer. 2001 Nov;32(3):203–11.

91. Brüderlein S, Sommer JB, Meltzer PS, Li S, Osada T, Ng D, et al. Molecular characterization of putative chordoma cell lines. Sarcoma. 2010;2010:630129.

92. Owen JH, Komarck CM, Wang AC, Abuzeid WM, Keep RF, McKean EL, et al. UM-Chor1: establishment and characterization of the first validated clival chordoma cell line. J Neurosurg. 2018 Mar;128(3):701–9.

93. Gellner V, Tomazic PV, Lohberger B, Meditz K, Heitzer E, Mokry M, et al. Establishment of clival chordoma cell line MUG-CC1 and lymphoblastoid cells as a model for potential new treatment strategies. Sci Rep. 2016 Apr 13;6(1):24195.

94. Hsu W, Mohyeldin A, Shah SR, ap Rhys CM, Johnson LF, Sedora-Roman NI, et al. Generation of chordoma cell line JHC7 and the identification of Brachyury as a novel molecular target. J Neurosurg. 2011 Oct;115(4):760–9.

95. Leibovitz A, Stinson JC, McCombs WB, McCoy CE, Mazur KC, Mabry ND. Classification of human colorectal adenocarcinoma cell lines. Cancer Res. 1976 Dec;36(12):4562–9.

96. Ma W, He L, Liu C, Zhang Q, Ding Y. [Establishment of a colorectal cancer SW620 cell line stably over-expressing Wilm's tumor on X chromosome using a recombinant lentivirus vector]. Nan Fang Yi Ke Da Xue Xue Bao. 2015 Aug;35(8):1122–7.

97. Niforou KM, Anagnostopoulos AK, Vougas K, Kittas C, Gorgoulis VG, Tsangaris GT. The proteome profile of the human osteosarcoma U2OS cell line. Cancer Genomics Proteomics. 2008;5(1):63–78.

98. Mahmood T, Yang PC. Western Blot: Technique, Theory, and Trouble Shooting. North Am J Med Sci. 2012 Sep;4(9):429–34.

99. CellEvent™ Senescence Green Detection Kit [Internet]. [cited 2022 Sep 13]. Available from: https://www.thermofisher.com/order/catalog/product/C10850

100. InCELL Target Engagement Assays - [Internet]. [cited 2022 Aug 19]. Available from: https://www.discoverx.com/products-applications/target-engagement-assays?gclid=EAIaIQobChMI8Nnm3erS-QIVaoBQBh1OgQD2EAAYASAAEgKEOPD_BwE

101. Concordet JP, Haeussler M. CRISPOR: intuitive guide selection for CRISPR/Cas9 genome editing experiments and screens. Nucleic Acids Res. 2018 Jul 2;46(W1):W242–5.

102. Workman P. Guidelines for the welfare and use of animals in cancer research. Br J Cancer. 2010;23.

103. Davis-Gilbert Z, Drewry DH, Hossain MA, Newman J, Gileadi O, Wells CI, et al. Covalent Data Screen of TBXTA-C006 [Internet]. Zenodo; 2022 [cited 2022 Dec 5]. Available from: https://zenodo.org/record/6629195

104. Bacon CW, D'Orso I. CDK9: a signaling hub for transcriptional control. Transcription. 2019 Apr;10(2):57–75.

105. Poon E, Liang T, Jamin Y, Walz S, Kwok C, Hakkert A, et al. Orally bioavailable CDK9/2 inhibitor shows mechanism-based therapeutic potential in MYCN-driven neuroblastoma. J Clin Invest. 2020 Nov 2;130(11):5875–92.

106. Kaufmann SH, Desnoyers S, Ottaviano Y, Davidson NE, Poirier GG. Specific proteolytic cleavage of poly(ADP-ribose) polymerase: an early marker of chemotherapy-induced apoptosis. Cancer Res. 1993 Sep 1;53(17):3976–85.

107. Egloff S. CDK9 keeps RNA polymerase II on track. Cell Mol Life Sci. 2021 Jul 1;78(14):5543–67.

108. Wang L, Doherty GA, Judd AS, Tao ZF, Hansen TM, Frey RR, et al. Discovery of A-1331852, a First-in-Class, Potent, and Orally-Bioavailable BCL-XL Inhibitor. ACS Med Chem Lett. 2020 Oct 8;11(10):1829–36.

109. Yosef R, Pilpel N, Tokarsky-Amiel R, Biran A, Ovadya Y, Cohen S, et al. Directed elimination of senescent cells by inhibition of BCL-W and BCL-XL. Nat Commun. 2016 Sep;7(1):11190.

110. Linardic CM. PAX3-FOXO1 fusion gene in rhabdomyosarcoma. Cancer Lett. 2008 Oct 18;270(1):10–8.

111. Huang M, Weiss WA. Neuroblastoma and MYCN. Cold Spring Harb Perspect Med. 2013 Oct 1;3(10):a014415.

112. Han H, Jain AD, Truica MI, Izquierdo-Ferrer J, Anker JF, Lysy B, et al. Small-Molecule MYC Inhibitors Suppress Tumor Growth and Enhance Immunotherapy. Cancer Cell. 2019 Nov 11;36(5):483-497.e15.

113. Bai L, Zhou H, Xu R, Zhao Y, Chinnaswamy K, McEachern D, et al. A Potent and Selective Small-Molecule Degrader of STAT3 Achieves Complete Tumor Regression In Vivo. Cancer Cell. 2019 Nov 11;36(5):498-511.e17.

114. Hu S, Marineau JJ, Rajagopal N, Hamman KB, Choi YJ, Schmidt DR, et al. Discovery and Characterization of SY-1365, a Selective, Covalent Inhibitor of CDK7. Cancer Res. 2019 Jul 1;79(13):3479–91.

List of figures

List of tables